WILEY-VCH

# Advances in rational designs and materials of high-performance stretchable electromechanical sensors

*Toan Dinh*, Thanh Nguyen, Hoang-Phuong Phan, Tuan-Khoa Nguyen, Van Thanh Dau, Nam-Trung Nguyen, Dzung Viet Dao*

Dr. T. Dinh, Mr. T. Nguyen, Dr. H.-P. Phan, Dr. T.-K. Nguyen, Prof. N.-T. Nguyen, Prof. D. V. Dao, Queensland Micro- and Nanotechnology Centre, Griffith University, Australia

Dr. T. Dinh, School of Mechanical and Electrical Engineering, University of Southern Queensland, Australia

Dr. V. T. Dau, Prof. D. V. Dao, School of Engineering and Built Environment, Griffith University, Australia

*E-mail: toan.dinh@griffith.edu.au; Toan.Dinh@usq.edu.au

Keywords: advanced materials, rational designs, stretchable sensors, electromechanical sensors, wearable applications

Stretchable and wearable sensor technology has attracted significant interests and created high technological impact on portable healthcare, and smart human-machine interfaces. Wearable electromechanical systems are an important part of this technology that has recently been witnessed tremendous progress toward high performance devices for commercialisation. Over the past few years, great attention has been paid to simultaneously enhance the sensitivity and stretchability of the electromechanical sensors toward high sensitivity, ultra-stretchability, low power consumption or self-power functionalities, miniaturisation as well as simplicity in design and fabrication. This review presents state of the art advanced materials and rational designs of electromechanical sensors for wearable applications. Advances in various sensing concepts and structural designs for intrinsic stretchable conductive materials as well as advanced rational platforms are discussed. In addition, the practical applications and challenges in the development of stretchable electromechanical sensors are briefly mentioned and highlighted.

## 1. Introduction

Stretchable electromechanical sensors are a class of highly deformable sensing devices that monitor a wide range of physical variables such as stress/strain, force and pressure [1-4]. Development and commercialization of these sensors have attracted considerable interest in wearable applications, where sensor wearability is vital for sensing the dynamic movement of curved surfaces and deformed objects [5, 6]. An effective solution is using stretchable intrinsic materials and stretchable structural designs to form mechanical sensors [7, 8]. Compared to conventional rigid sensors, it is desirable for stretchable sensors to provide mechanical robustness, biocomparability, multifunctionality, as well as comfort of wearing such sensors [9, 10]. Stretchable electromechanical sensors are capable of being comfortably attached on the human body and skin and perceiving mechanical stimuli. These sensors have huge potential applications in personal healthcare, including detection of human motion/gesture, breath and pulse monitoring. Stretchable electromechanical sensors have recently attracted great interest due to their high sensitivity, stretchability, simplicity in design and implementation. Compared with the other kinds of sensors, e.g. stretchable piezoelectric/triboelectric sensors, electromechanical sensors usually require supply power or battery.

A stretchable sensor typically consists of a sensing block embedded or integrated into a stretchable substrate that can be elongated under application of mechanical stimuli [11, 12]. The sensing block acts as a mechanical sensing unit, which for instance converts stress/strain into a measurable electrical signal. The presence of nanomaterials and composites in the sensing block has been utilized as a preferable design for stretchable sensors [11, 13]. Selection criteria of these materials include structural stretchability, suitable conductivity and high mechanical strength. Designing the sensing structure aims for high sensitivity, fast response, linearity and a wide working range [14, 15]. The integration of nanomaterials and nanocomposites into stretchable sensors are currently an emerging trend of wearable sensors in their research,

development and commercialisation [10, 11]. The development of stretchable sensors with low power consumption for portable applications is also of great interest [16, 17].

The conventional design method for "partly stretchable" sensing devices integrates "hard" sensors and "soft" interconnects to form "island-interconnect" configurations [18, 19]. This approach deploys an isolated island to carry the rigid sensors and a stretchable network of interconnections. Geometric engineering structures including serpentine and fractal designs have been widely employed, to achieve stretchability for the interconnections [20]. This method inherits the advantages of conventional sensors while adding a new important stretchability feature to the system [21]. However, the stress concentration within the sensors limits the applications of this approach. "Fully stretchable" sensors enable the collection of mechanical stimuli generated in a wide range of wearable applications [8, 22]. The design of this type of sensors requires stretchability of the whole system including stretchable sensing blocks and stretchable substrates. This process involves the integration of different materials and fabrication strategies for electrodes, dielectrics and sensors. The most challenging task is selecting materials for the design of a sensing mechanism to achieve high-performance sensors with tuneable conductivity [23], high sensitivity [24, 25] and linearity [26] in a wide range of applied strain, and low power consumption or zero power consumption [16, 27].

Recently, advancements in data processing of electromechanical sensor signals have also been made with a view to wireless communication [28]. Wireless technology has been employed to enable stretchable electromechanical sensors portability and conformability for wearable applications [29]. This technology typically deploys the integration of capacitance and inductance in the same platform with electromechanical sensors. In addition, the change of capacitance or inductance to mechanical stimuli will result in shifts of the resonant frequency that is an indicator for qualifying the amplitude of the mechanical input [30]. Advanced designs of wireless based stretchable electromechanical sensors will take advantage of the wireless technology to wearable sensing applications.

This paper summarises the development of advanced materials and structural designs for stretchable electromechanical sensors, including strain and pressure sensors toward high performance and ultra-stretchability. We firstly focus on new principles and structural designs of electromechanical sensors, including the recent advances in sensing concept of stretchable strain/pressure sensors based on the changes of resistance (Section 2) and capacitance (Section 3) to mechanical stimuli. Examples of sensing concepts are strain-induced tunable conductivity of stretchable sensors via piezoresistance and contact-based tunable resistance in intrinsic stretchable nanomaterials and nanocomposites. In Section 4, we introduce stretchable mechanical sensors based on the coupling of capacitance and inductance, and the development of low powered consumption sensors using stretchable conductors for wearable applications. In terms of material designs (Section 5), we discuss the significance of intrinsic stretchable materials such as ionic liquid, liquid metals and conductive polymer for mechanical sensors. Recent developments of advanced nanocomposites and other materials are also reviewed. Different to some reviews on stretchable sensors and electronics [11, 12, 14, 31-33], we focus on the modern trend and the most recent progress in the development of advanced materials and rational designs of stretchable electromechanical sensors towards high performance devices. This review provides insights into how to design appropriate structures and select suitable materials for stretchable electromechanical sensors. The paper also produces useful guidance for material and structural designers in terms of high sensitivity and ultrastretchability (**Figure 1**). Notably, the development of new 2D materials (e.g. Mxene) with binding materials have led to exceptionally high sensitivity (GF=8,700) [34] and stretchability (3400%) [35]. Novel transferred strategies enable hard and superior robust materials, e.g. silicon carbide (SiC) to a flexible and stretchable platform, opening new opportunities for applications with harsh environments including implantable devices and high temperature sensing systems.

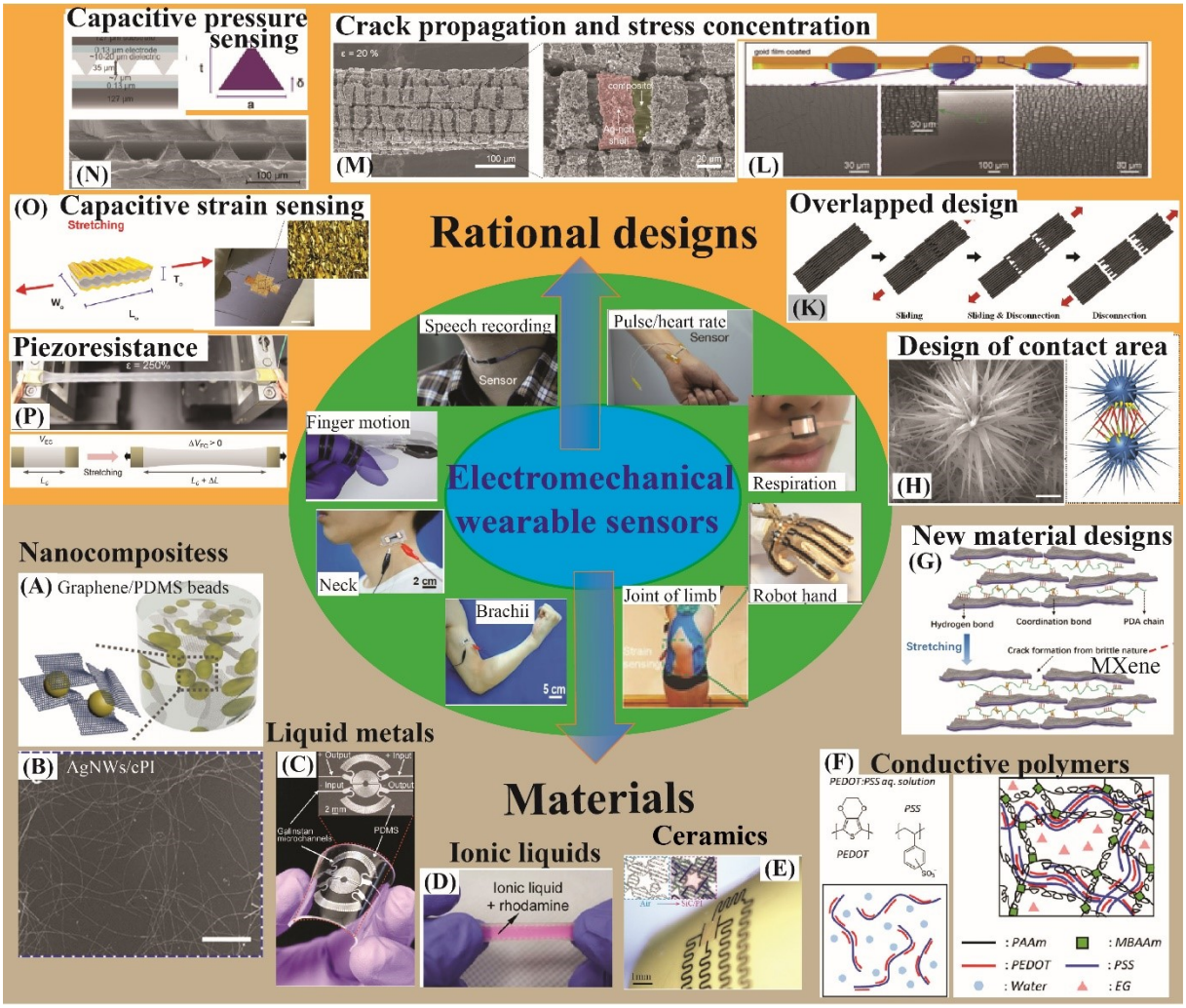


**Figure 1**. Advanced materials and rational designs of electromechanical sensors for wearable applications. Materials: (A) Nanocomposite-Graphene/PDMS beads. [36] Copyright 2019, Elsevier. (B) Silver nanowires/colorless-polyimide (AgNWs/cPI). [37] Copyright 2019, American Chemical Society. (C) Liquid metals. [38] Copyright 2017, Willey-VCH. (D) Ionic liquids. [39] Copyright 2017, American Chemical Society. (E) Transferred materials. [4] Copyright 2019, American Chemical Society. (F) Conductive polymers. [40] Copyright 2016, Willey-VCH. (G) New material designs. [34] Copyright 2019, American Chemical Society. Rational designs: (H) Design of contacting surface areas. [41] Copyright 2018, Nature Publishing Group. (K) Overlapped design. [42] Copyright 2019, Wiley-VCH. (L) Stress concentration. [43] Copyright 2019, Willey-VCH. (M) Crack propagation. [44] Copyright 2018, American Chemical Society. (N) Capacitive pressure sensing. [45] Copyright 2019, Wiley-

VCH. (O) Capacitive strain sensing. [46] Copyright 2018, American Chemical Society. (P) Piezoresistance. [39] Copyright 2016, American Chemical Society. Wearable applications: Detection of movement of neck and biceps brachii. [47] Copyright 2018, Wiley-VCH. Monitoring movement of joint of lower limb. [48] Copyright 2018, Willey-VCH. Movement of robot hand. [49] Copyright 2019, Wiley-VCH. Measuring human respiration. [50] Copyright 2018, American Chemical Society. Pulse/heart rate measurement and human speech recording. [51] Copyright 2014, Nature Publishing Group. Detection of finger motion. [52] Copyright 2018, AAAS.

**2. Resistive stretchable sensors**

Resistive sensors refer to a class of electromechanical sensors that use resistance change as an indicator for the magnitude of the input signals. Resistive electromechanical sensors convert mechanical deformation/signals (i.e. stress/strain and pressure) into an electrical signal, which is evaluated via the electrical resistance. Stretchable resistive sensors have attracted significance interest owing to their simplicity in design, fabrication and measurements. The sensing mechanism of resistive sensors is typically categorised into two main groups of piezoresistance and contact-based resistance. In piezoresistive sensors, the resistance of a sensor is defined as, $R=\rho\frac{L}{wt}$, where ρ is the electrical resistivity; $L$, $w$ and $t$ are the length, width and thickness of the sensor, respectively. The common approaches of forming a resistive sensor are to (1) deposit a conductive network of nanomaterials/nanocomposites on top of a stretchable substrate, or (2) to uniformly embed the material in the substrate. The sensitivity of the sensor is known as the gauge factor $GF= \Delta R/R_o \times 1/\varepsilon$, defined from the slope of the relative resistance change ΔR/Ro to the applied strain ε. The stretchability of electromechanical sensors is quantitatively measured by maximum applied strain ($\varepsilon = \Delta L/L_o \times 100\%$ where $L_o$ and $\Delta L$ are the original length and the incremental length, respectively) without causing damages or degradation of the mechanical and electrical properties of the sensors. For wearable physical sensing, including

detection of human motion, arm, armpit, and knee, the requirements for stretchability is typically lower than 55%. However, high stretchability is preferable for a wide range of applications. Under a small applied strain (e.g. <1%), the GF value mainly comes from the geometric change in metals and resistivity change in semiconductors. The GF value is limited by the natural properties of piezoresistive materials. For example, GF was found to be approximately 2-3 for metals, -125 to 200 for silicon and -30 to 30 for polysilicon [53]. Piezoresistive sensors can be designed in a form of stretchable patterns such as serpentine and mesh, to avoid cracks and damages at higher applied strain.

In a contact-based resistive sensor, the electrical resistance of the sensor $R$ comes from the resistance of the conductive parts/blocks ($R_m$) and the contact/tunnelling resistance between them ($R_c$), where the change of ($R_c$) is dominant under the applied strain. Therefore, the GF value of stretchable mechanical sensors based on contact resistance could be very large. However, the working range of these stretchable sensors is limited by increasing resistance with tensile strain. This type of sensor employs contact resistance-based transduction mechanisms, including overlapped area between conductive blocks, crack-induced changes in the resistance, tunnelling distance and stress-concentration induced resistance changes. The following sections will discuss the recent advances in the development of resistive strain and pressure sensors based on piezoresistive, overlapping-based, crack-based and stress-concentration mechanisms.

### 2.1. Stretchable strain sensors

This section presents three main kinds of mechanisms used for stretchable strain sensors, namely piezoresistance, overlapping-based sensing and crack-based concept. Piezoresistive strain sensors employ the change of resistance in corresponding to the change of the sensor geometry and resistivity, where the geometry change is dominant. This kind of sensor is typically made from intrinsic stretchable materials, including ionic liquids, liquid metals and conductive polymers. Piezoresistive strain sensors have high stretchability (>300%), but a low

sensitivity that is limited by the natural sensing properties of the materials. In addition, overlapped-based and crack-based strain sensors operate based on the contact area and gap, respectively, between conductive blocks. These kinds of sensors offer a high sensitivity while their stretchability is restricted by the initial contact area in overlapped-based sensors and the density of microgaps/microcracks in crack-based sensors.

*2.1.1. Piezoresistive strain sensors*

In piezoresistive stretchable strain sensors, the resistance change is given by $\Delta R/R_o = (1+2v)\varepsilon + \Delta\rho/\rho o$, where $(1+2v)\varepsilon$ is the resistance change due to geometric/dimension change ($v$ is the Poisson's ratio) and $\Delta\rho/\rho o$ is the resistivity change by the relocation of charge carriers and/or the change in the number of carriers under applied strain ε. In a number of intrinsic materials, the change of resistance corresponding to the applied strain depends on the geometric change, **Figure 2**A. This section discusses the recent development of piezoresistive strain sensors based on this effect.

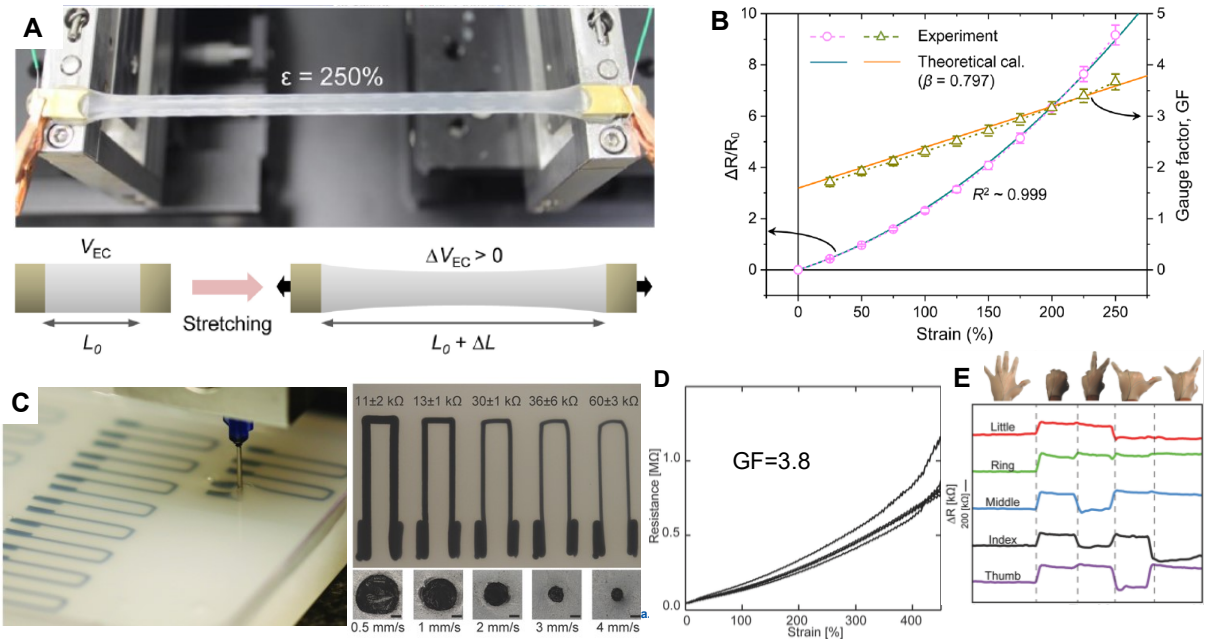


**Figure 2:** Stretchable strain sensors based on piezoresistance of soft conducting-materials. (A) Stretchability of ionic liquid strain sensors embedded in ecoflex. The volume of the elastomeric channel increases when the channel is stretched. (B) Gauge factor of less than 4 was measured for the ionic liquid piezoresistive sensors. [39] Copyright American Chemical Society 2016.

(C) 3D printing of conductive carbon grease. (D) Electrical resistance as a function of strain up to 450% strain with a GF of 3.8. (E) Electrical resistance vs. time for piezoresistive sensors integrated in a glove at five different hand gestures. [54] Copyright 2014, Wiley-VCH.

From the material perspective, conductive liquids such as ionic liquids and liquid metals have attracted great interest toward artificial skin and wearable applications [55, 56]. The change in the geometry of liquid metals or ionic liquids embedded in elastomeric channels has been utilised for piezoresistive stretchable strain, pressure and force sensors [57, 58]. The density of conductive pathways decreases with increasing applied tensile strain or elongation. Figure 2B shows the sensitivity of ionic liquid piezoresistive sensors that have resistance changes depending upon the geometrical changes. Although these liquid strain sensors exhibit relatively low GF of less than 4, they can experience a broad range of tensile strain of up to 400%, suitable for epidermal applications, Figures 2B and D. Furthermore, liquid based sensors take advantage of the 3D-printing technology to enable device miniaturization and multiple-device integration, shown in Figure 2C. The main advantages of these sensors are the high stretchability and suitability for attachment on complex 3D- shapes and curved surfaces [3, 59]. The simplicity in design and implementation enables conductive liquid sensors to be fabricated on a dense array of sensors in a small area. Therefore, these sensors have been used to measure hand motions, body motions and other wearable devices [60]. However, these sensors typically show hysteresis and large drift as deformation increases due to the permanent change in the conductive network or material structures [38, 54, 61] (Figure 2E). The stretchable sensors solely based on liquid conductors typically have high conductivity and this makes the wiring/interconnections more challenging to distinguish the sensing effect with the contact resistance changes or resistance change of soft wires [61]. The combination of a liquid and a conductive filler can enhance the sensitivity by inducing cracks or disconnections under large

applied strain. This results in a higher sensitivity of 25.2 for ionic liquid/graphene [62] and 31.6 for rGO (reduced graphene oxide)/DI (deionized water) [63].

*2.1.2. Overlapping-based strains sensors*

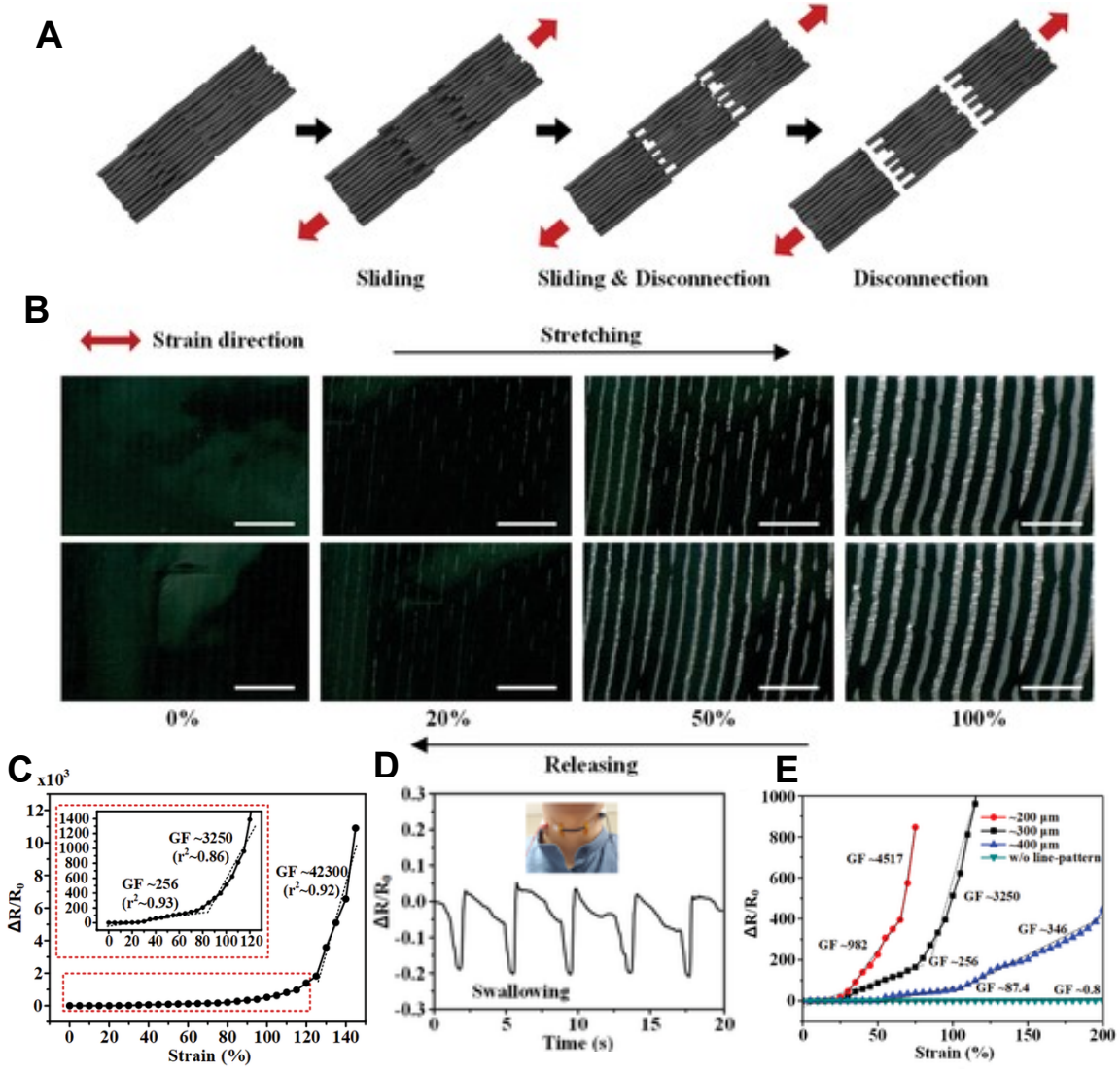


**Figure 3**: Stretchable sensors based on contact resistance of conductive blocks. (A) Sliding and disconnections between the CNTs blocks. (B) Optical images of CNT strain sensors under stretching conditions of up to 100%. (C) Resistance change vs. strain showing a large GF of up to 42300. (D) Resistance response to wrist pulse. (E) Resistance response to swallowing. (A)-(E) Reproduced with permission. [42] Copyright 2019, Wiley-VCH.

The resistance of strain sensors can change with the sliding or overlapped area between the nanomaterial blocks. This type of sensors has been developed towards high sensitivity. For example, **Figures 3**A and B highlight the structural design of overlapped carbon nanotubes (CNTs) embedded in ecoflex [42]. Under tensile stretching conditions, the overlapped areas between CNT blocks decrease and are separated, leading to disconnections of the electrical pathways. The disconnection mechanism is insignificant with GF of 256-3,250 at a low stretching range of 0-125%, while showing a high sensitivity (GF=42,300) at a large strain range (125-140%) (Figure 3C). The high sensitivity and stretchability allowed the CNT overlapping sensor to be affixed to human skin and measure the human motion in real-time for applications such as twist pulse detection (Figure 3D). Other nanomaterials including graphene oxide (rGO) and metal nanowires (e.g. AgNWs) have been intensively employed in the design of overlapped strain sensors. Compared to the CNT sensors, the sensitivity of other overlapped sensors is much lower (e.g. a GF value of up to 150 for rGO embedded in the VHB stretchable tape [64], and GF~14 for AgNWs-PMDS strain sensors [2]). The sensitivity can be improved by decreasing the size of the conductive blocks and lowering the density and thickness of the nanomaterials. For example, shorter CNT overlapped areas showed more rapid increase in the electrical resistance but have a lower operating range (Figure 3E). In general, higher sensitivity leads to a narrower working range of the applied strain. The long-term stability of thousands of testing cycles has been successfully demonstrated without significant degradation of the sensor response [42, 65, 66]. **Table 1** lists the recent advances in the development of stretchable strain sensors based on three main sensing mechanisms: piezoresistance, overlapping/ disconnection and crack propagation.

**Table 1**. Recent progress on materials and designs of stretchable strain sensors

| Mechanism | Materials | Gauge factor | Stretchability | Ref. |
|---|---|---|---|---|
| Piezoresistance | EGaIn/silicone elastomer | 0.97-4.17 | 0%-100% | [61] |
| | PEDOT:PSS hydrogel | 0.5 | 0-300% | [67] |
| | Ionic liquid/PDMS | 2-2.8 | 0%-80% | [68] |
| | CNT/PDMS | 0.82 | 0-10% | [69] |
| | | 2.21 | 10%-80% | |
| | | 6.44 | 80%-100% | |
| | GaInSn/PDMS | ~3 | 0%-50% | [60] |
| | CNT−polymeric core fibers | −0.063 | 0%-25% | [70] |
| | | 0.68 | 50%-100% | |
| | | 1378 | 300%-330% | |
| Overlapping | CNT/ecoflex | 256 | 0%-80% | [42] |
| | | 3250 | 80%-125% | |
| | | 42300 | 125%-140% | |
| | GnPs/PDMS | 27.7–164.5 | 0%-12% | [65] |
| | Ternary nanocomposite | Up to 2392.9 | Up to 62% | [66] |
| | Graphene armour scales | Up to 1054 | Up to 26% | [71] |
| | Graphene oxide/VHB | 16.2 | 0%-60% | [64] |
| | | 150 | 60%-82% | |
| | AgNW/PDMS | 2-14 | 0%-70% | [2] |
| | graphene flakes/ZnO/PDMS | 13.3 | 0%-30% | [72] |
| Crack | RGO/ Polyurethane (PU) | 205-3256 | 0%-180% | [73] |
| propagation | Mxene/PET and PDMS | ~20 | 0%-40% | [52] |
| | MWCNT/PDMS | 56 | 0%-70% | [74] |
| | CNT films/PDMS | 87 | 0%-40% | [75] |
| | | 6 | 40%-100% | |

| | | | | |
|---|---|---|---|---|
| | Graphene flakes/porous pad | 2-160 | 0%-350% | [76] |
| | CNT/PDMS | 35.75 | 0%-45% | [77] |
| | Ag nanoparticles coated on stretchable fiber | 182 | 0%-60% | [44] |
| | | 1032 | 60%-100% | |
| | | 104 | 150%-200% | |
| | | $3.1\times10^4$ | 200%-260% | |
| | | $9.3\times10^5$ | 350%-450% | |
| | CNT/ KH550/PMDS | 5-1000 | 2%-250% | [78] |
| | Au micromesh/PDMS | $10^8$ | 0.02%−4.5% | [79] |
| | Graphene ink/ PDMS | 1054 | 0%−26% | [71] |
| | Graphite/Ecoflex (Short cracks) | 522.6 | >50% | [80] |
| | Graphite/Ecoflex (Long cracks) | 11344 | <50% | |
| Percolation network | AgNWs/PDMS | 846@150% | 0%−150% | [81] |
| | AgNWs/PDMS | 150,000 | 0%−60% | [82] |
| Piezoresistive-crack hybrid | Graphene/Glycerol-KCl/Ecoflex | 25.2 | 0%-300% | [62] |

*2.1.3. Crack-based strains sensors*

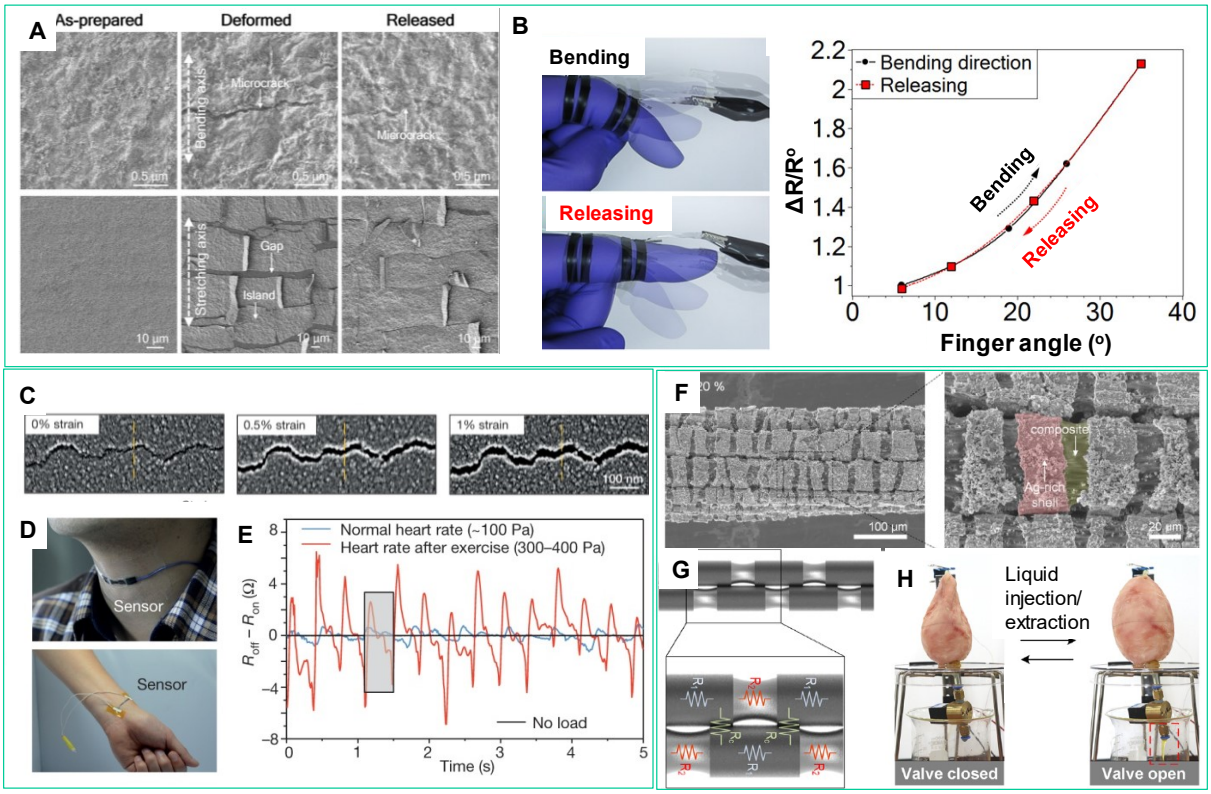


**Figure 4**. Cracked strain sensors. (A) Cracks occur in conductive MXene in PET (bending) and PDMS (stretching). (B) MXene wearable strain sensor for detection of human motion with resistance change vs finger motion. [52] Copyright 2018, AAAS. (C) Cracks in Pt films on polyurethane acrylate under applied strain. (D) Wearable applications of Pt-cracked films and (E) Resistance change vs heart rates. [51] Copyright 2014, Nature Publishing Group. (F) Crack-based multifilament fibre strain sensors. (G) Resistance model of the fiber strain sensor with two filaments and the corresponding equivalent circuit. (H) Photographs of the operation of the artificial bladder system using the fibre strain sensor on the pig bladder. [44] Copyright 2018, American Chemical Society.

Cracked microstructures of nanofilms and composites have been demonstrated as an effective approach to improve the sensitivity of stretchable strain sensors. As such, the reversible resistance change of strain sensors can be qualified by the value of gauge factor, which represents the propagation of cracks in the micro/nanostructures. The conductive pathways of

materials are typically affected by a small applied strain, leading to a large change in the electrical resistance and a large GF. The conventional design approach for stretchable strain sensors is using crack propagation in metal nanoparticles, metal nanowires, graphene and carbon nanotubes (CNTs) which are coated or embedded into flexible and stretchable substrates [83, 84]. Because of high flexibility and excellent electrical conductivity, these nanomaterials have been employed in applications such as monitoring of physiological signals to vigorous motions. More recently, two dimensional nanomaterials including conductive MXene with stretchability, bendability and foldability have been demonstrated for large scale mechanical deformation and utilised for bending and stretching in wearable applications. **Figures 4**A and B show the propagation of gaps/cracks in the MXene films under bending and stretching conditions and the reversible resistance when detecting the motion of human fingers. Initial bending and stretching was utilised to create microcracks and gaps which are not very large to destroy the connections between conductive blocks. Stretching enables the open and close/recover of the microcracks which control the conductivity of the MXene films. The same sensing mechanism has been employed for CNT stretchable strains sensors [1] and organic-based semiconductors [85]. For example, Figure 4C shows the propagation of microcracks in Pt-based film strain sensors under stretching and Figures 4D and E illustrate the application of these sensors in wearable physical sensing and monitoring of human pulse [51]. Fibre strain sensors have also attracted great interest due to the high potential stretchability, excellent electrical conductivity and wide sensing range. Notably, thanks to the cracks-propagation mechanism, the recent development of Ag nanoparticles-coated on multifilament fibres [44] shows the high-performance cracks-based fibre sensors (Figure 4F) with a gauge factor of ~10^6 in a broad range of strain (200%) with high durability (10,000 cycles). The contact model with equivalent circuit in Figure 4G indicates the contribution of electrical contact between the Ag conductive blocks under stretching. In addition, applications for an artificial bladder system using the fibre strain sensor on a pig bladder was also successfully demonstrated (Figure 4H).

In terms of structural design, initial cracks and crack densities (i.e. discontinuous gaps per unit area) can be introduced by pre-stressing and releasing. Complex strains can be generated by various structural designs in the strain sensors during stretching, leading to the complex distributions of produced cracks and control of the strain sensitivity. Typically, the stretchability of crack-based strain sensors is proportional to the density of cracks while the sensitivity decreases with increasing crack densities. For example, Song et al. [86] reported the metal film/elastomer strain sensors with a high crack density. These sensors have a GF of up to 475 and a limitation for the stretchability of 30%. Gupta et al. [79] demonstrated a record GF of 108 in 0.02%−4.5% strain for a crack-based strain sensor with Au microwire network semi-embedded in a PDMS matrix. In addition, great effort has been paid to reconcile the conflict between achieving a desirable high sensitivity and a broad working range of stretchable strain sensors [87]. The repeatability and a long-term stability of crack-based electromechanical sensors have been also demonstrated up to a few thousand testing cycles [73].

*2.1.4. Percolation network based sensors*

Design of the percolation network, including metal nanowire composites, offers high conductivity, flexibility and high potential for stretchable electromechanical sensors [81,82], electronics [88-90] and energy harvesters [91,92]. For example, AgNWs percolation networks based on the mesh structured substrate [81] have been demonstrated with low sheet resistance of 14.9 Ω/sq, high stretchability of 150%, high transparency of 88.3% and high sensitivity of GF=846. Under large applied strain, the conductive networks are cracked locally and these microcracks are blocked by the conducting paths, resulting in an increase in electrical resistance with increasing tensile strain [81]. This microcrack-assisted mechanism in percolation networks of AgNWs has been employed to develop ultrasensitive strain sensors with a record GF of 150,000 and large stretchability of 60% strain [82].

*2.1.5. Smart structural designs of stretchable electromechanical sensors*

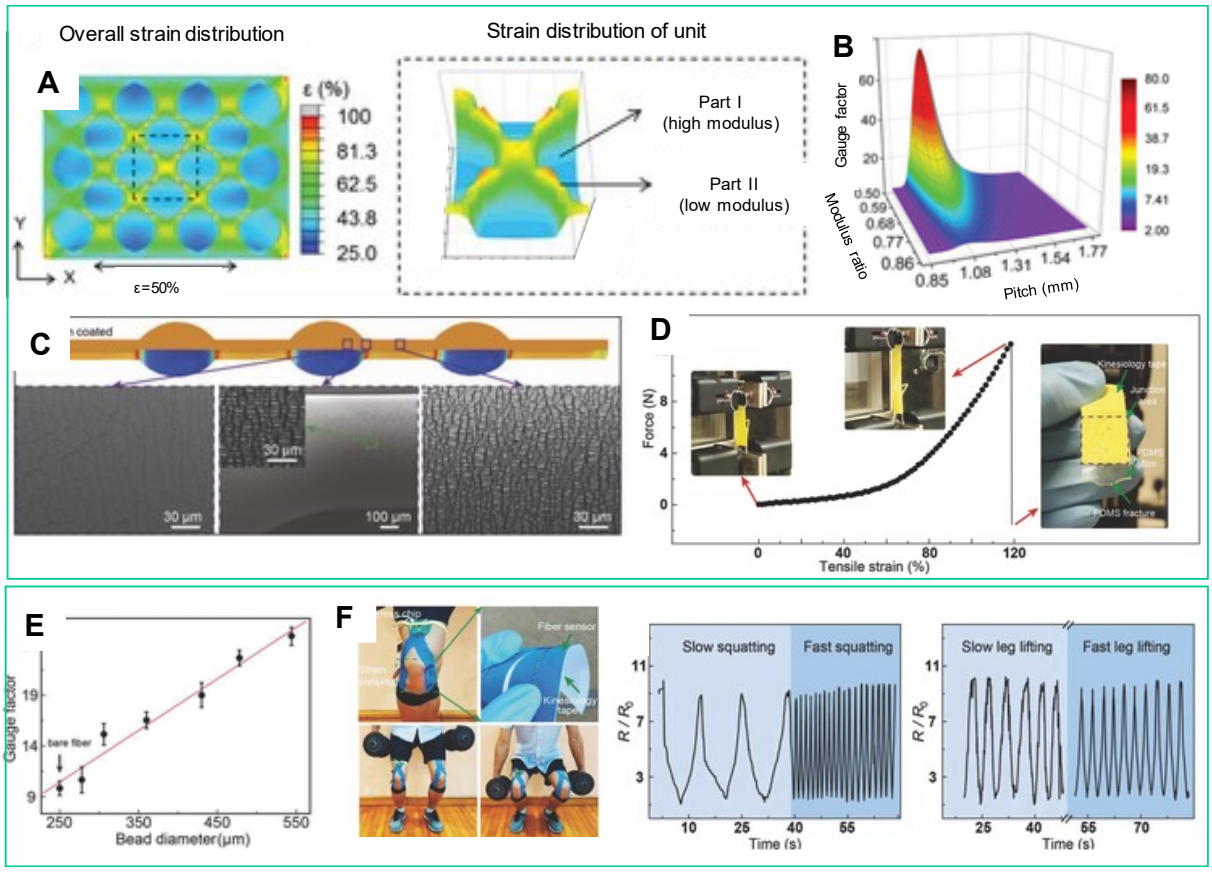


Figure 5: Enhancement of strain sensitivity by mechanical design of strain concentration. (A) Strain distribution (left) in heterogeneous substrates and concentration (right) based on the design of the high modulus and low modulus parts. (B) Contour map of the sensitivity vs pitch and modulus ratio. [43] Copyright 2019, Willey-VCH. (C) Concentration of surface strain for the sensitivity enhancement of fiber-based stretchable strain sensors. (D) Adhesion test of integrated fiber sensor into PDMS film. (E) Gauge factor vs dead diameter. (F) Sensor affixed on the joint of lower limb to measure squatting and leg lifting. [48] Copyright 2018, Willey-VCH.

Applications of stretchable strain sensors require a different range of strain, and there is a trade-off between the stretchability and the sensitivity of these sensors. The high interests in developing resistive strain sensors with high performance led to the need of customising the sensitivity. Redistribution of strain has been proposed as an effective method to enhance and

optimise the sensitivity of strain sensors. For example, **Figure 5**A shows the strain distribution on the heterogeneous substrate (2-dimentional design of sensors). The area with lower Young modulus is under a higher strain concentration that results in a higher disruption in the conductivity under applied strain. The sensitivity can be tuned by changing the centre-to-centre distance of high-modulus adjacent parts and the ratio of low to high Young's modulus (Figure 5B). In another work [48], surface strain is redistributed on microfibres to enhance strain sensitivity (Figure 5C). Intrinsic microbeads are added to induce strain/stress concentration in the area with geometry/size changes where the microcracks occurred and are developed. This modified structure can be embedded into PMDS films with high mechanical robustness (Figure 5D). The sensitivity increases with increasing size of the micro beads as the cracks are longer and wider at the area with concentrated strain, Figure 5E. This area defines the resistance change in the design with higher sensitivity compared with design of no microbeads. This sensor can be adhered to the human joint and measure the squatting/lifting, indicating the high potential for wearable sensing applications, Figure 5F.

### 2.2. Stretchable pressure sensors

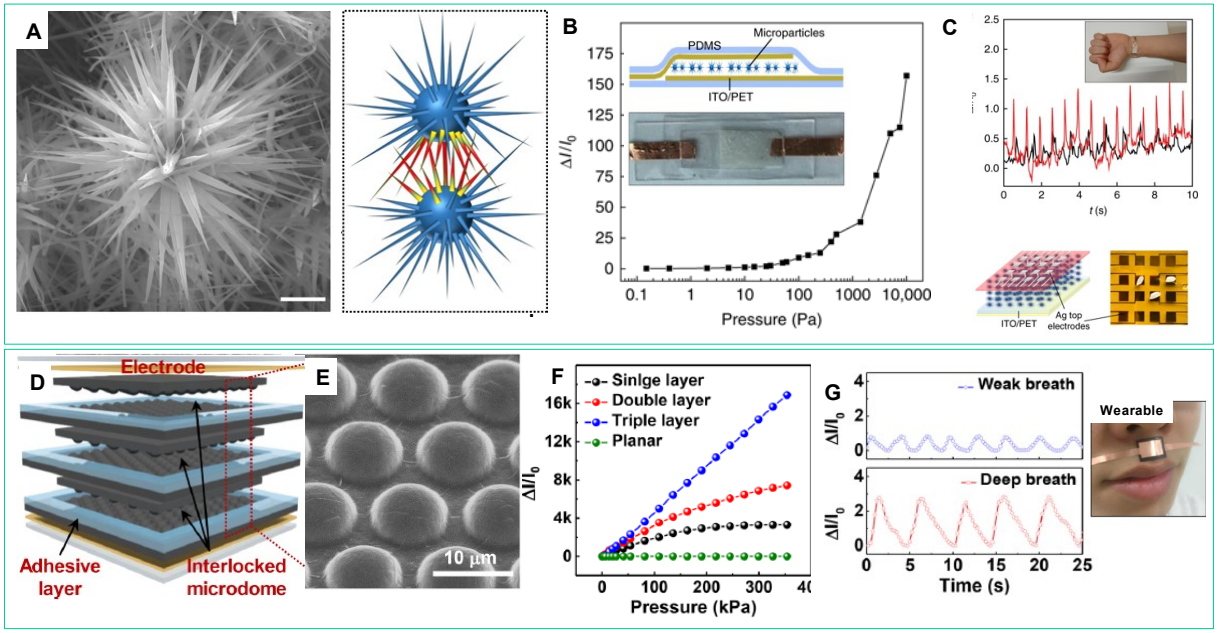

Figure 6. Piezoresistive pressure sensors. (A) High-magnification SEM image of one sea urchin-shaped microparticles (SUSM), showing a forest of nanostructured spines. (B) Measured current vs pressure (0-10 kPa). The inset shows the structure of the pressure sensor and optical image of the sensors. (C) Measured pulse signals from the wrist. The black curve shows a normal heart rate and red curve was measured after exercise. Capability of fabricating arrays of SUSM devices. [41] Copyright 2019, Springer Nature. (D) Schematic of multilayer e-skins with microdome-patterned rGO/PVDF composite film. (E) SEM image of the image of a microdome array. (F) Response of the sensor to the applied pressure. (G) Application of SUSM in measuring human respiration. [50] Copyright 2019, American Chemical Society.

Wearable resistive pressure sensors are of interest for applications in monitoring human physiological activities and artificial intelligent systems. These sensors mimic the response of human skin by detecting the change in applied pressure. Transduction mechanisms of piezoresistance, capacitance, piezoelectricity and triboelectricity have typically been employed. Among them, resistive-based pressure sensors use the change in electrical resistance in response to the change of pressure, depending on the designs of geometry, contact area and tunnelling capability of electrons. Conventionally, flexible resistive pressure sensors employ composite materials with planar designs, which exhibit poor sensing characteristics. In recent years, resistive pressure sensors with novel geometric micro/nanostructures have attracted great attention due to their high sensitivity and the simplicity in design and implementation [9]. Numerous interesting nanomaterials and smart structures have been designed with a view to outstanding performance in a broad range. These designs include a network of percolative nanomaterial blocks [87], interlocked mechanisms [93], porous networks [94-96], conductively coated micro/nanofibers [97] and other patterns [98, 99]. For example, **Figure 6**A shows the sea urchin-shaped microparticles (SUSM) with a forest of nanostructured spines [41]. This structure enables signal amplification to applied pressure via resistive inter-spine contacts and

piezoresistive spine bending of the SUSM. Figure 6B shows the SUSM-based pressure sensors with its ultrasensitive response of 121 $kPa^{-1}$ to applied pressure of up to 10 kPa and ultralow detection limit of 0.015 Pa and fast response of 7ms. This sensor can detect pulse signals from the wrist and is designed in an array for multiple sensing (Figure 6C). Notably, Lee et al. [50] designed multiple layer stacked structures of microdome-patterned rGO/PVDF composites, to broaden the sensing range at high sensitivity level (Figures 6D&E). Multiple layers showed tremendous enhancement in the sensitivity (Figure 6F) and enabled the development of respiratory devices (Figure 6G). Overall, the design of small area of initial contacts (e.g. point contact rather than line contact) can enhance the sensitivity to applied pressure and the detection limit [100]. In addition, the design of smart textile structures also allows the development of high-performance pressure sensors in wearable electronics [97]. **Table 2** summarises the various materials and designed structures utilised in resistive pressure sensors in recent years.

**Table 2**. Materials and designs for high-performance stretchable pressure sensors

| Materials & structures | Sensitivity | Pressure range | Stretchability | Number of cycle test | Ref. |
|---|---|---|---|---|---|
| CNT/NPCs/PDMS | >300 | 1Pa-25 kPa | | | [95] |
| rGO wrinkles | 47.5 $kPa^{-1}$ | 0 Pa–100 Pa | | | [101] |
| | 178 $kPa^{-1}$ | 100–200 Pa | | | |
| | 43.9 $kPa^{-1}$ | 200–500 Pa | | | |
| | 7.94 $kPa^{-1}$ | 500–3000 Pa | | | |
| Thixotropic inks (nanoclay, CB, and TPU) | 5.5 $kPa^{-1}$ | 0−10 kPa | 0%-80% | 1000 | [102] |
| | 0.43 $kPa^{-1}$ | 10−30 kPa | | | |
| | 0.0095 $kPa^{-1}$ | 30−440 kPa | | | |
| Graphene film/PET | 10.39 $kPa^{-1}$ | 0 – 2 kPa | 0%-5% | 1100 | [103] |
| | 0.0034 $kPa^{-1}$ | 2 – 200 kPa | | | |

| | | | | | |
|---|---|---|---|---|---|
| CNT/PDMS | 1.82 $kPa^{-1}$ or 0.107 $kPa^{-1}$ | 0-80kPa | - | 6000 | [100] |
| PEDOT:PSS/ AgNWs/ Ecoflex | 6.13 $kPa^{-1}$ | 0-90kPa | 0%-30% | 12000 | [104] |
| MXene@chitosan (CS)@polyurethane (PU) sponge | 0.014 $kPa^{-1}$<br>-0.015 $kPa^{-1}$<br>-0.001 $kPa^{-1}$ | 0-6.5 kPa<br>6.5-85 kPa<br>85-250 kPa | 0%-85% | 5000 | [94] |
| Graphite/ (G/PDMS) | 245 $kPa^{-1}$<br>90 $kPa^{-1}$ | 0–120 kPa<br>120–150 kPa | - | 25000 | [105] |
| rGO@PolyHIPE foams | 2.53 $kPa^{-1}$<br>0.21 $kPa^{-1}$<br>0.06 $kPa^{-1}$ | <0.14 kPa<br><120 kPa<br><200 kPa | - | 10000 | [106] |
| MXene (Ti3C2) nanosheets/cellulose | 12.5 $kPa^{-1}$ | 0-11kPa | 0%-95% | 10000 | [107] |
| MXene (Ti3C2) nanosheets/chitosan | 80.4 $kPa^{-1}$ | 0-5 kPa | 0.5%-70% | 150,000 | [108] |
| rGO aerogel/rGO paper | 349-253$kPa^{-1}$ | <1.4 Pa | 0%-90% | 10000 | [109] |
| Polypyrrole (PPy) hollow microspheres | 11.3 $kPa^{-1}$ | 0-180 Pa | - | 2500 | [110] |
| MXene-sponge/ PVA nanowires | 147 $kPa^{-1}$<br>442 $kPa^{-1}$ | <5.37 kPa<br>5.37-18.56 kPa | 0%-95% | 10000 | [98] |
| Hierarchical nanocomposite film | 0.036 $kPa^{-1}$ | <3 kPa | 0%-0.4% | 10000 | [99] |
| MWNT− | 0.022 $kPa^{-1}$ | <2.7 kPa | 10%-70% | 5000 | [96] |

| | | | | | |
|---|---|---|---|---|---|
| rGO@PU foam | 0.088 $kPa^{-1}$ | <11 kPa | | | |
| | 0.034 $kPa^{-1}$ | <50 kPa | | | |
| Wrinkled CNT thin | 278.5 $kPa^{-1}$ | 0-2Pa | 0%-67% | 500 | [111] |
| film electrodes | 13.2 $kPa^{-1}$ | 2–25 Pa | | | |
| Microarrays | 196 $kPa^{-1}$ | 0-100kPa | - | 10000 | [112] |
| of polystyrene | | | | | |
| PVDF/rGO | 47.7 $kPa^{-1}$ | 0-350 kPa | - | 5000 | [50] |
| Graphene/polyamide | 2.34 $kPa^{-1}$ | 0-80 kPa | 0%-100% | 10000 | [93] |
| interlocking fabric | | | | | |
| Graphene electrodes | 0.33 $kPa^{-1}$ | <1 kPa | - | 1000 | [113] |
| & Nylon netting | 0.007 $kPa^{-1}$ | <5kPa | | | |
| Zinc oxide / | 121 $kPa^{-1}$ | 0.015 Pa | 0%-0.82% | 2000 | [41] |
| biological bristles | | | | | |
| CNT-coated | 14.4 | 0-3.5 kPa | 0%-5.2% | 1000 | [97] |
| cotton fabric | 7.8 | 3.5-15 kpa | | | |

## 3. Capacitive stretchable sensors

As discussed in Section 2, resistive sensors have been widely employed thanks to their high sensitivity. However, these sensors have faced great challenges in practical applications due to their large hysteresis and non-linear response. In contrast, capacitive stretchable sensors have great linearity and a low degree of hysteresis, while suffering from low sensitivity. The sensitivity is defined by the capacitance change to applied strain and known as gauge factor $GF=\Delta C/C_o \times 1/\varepsilon$. Theoretically, the best sensitivity limit of these sensors is 1 for planar capacitive based strain sensors. High sensitivity of strain sensors is a desirable feature as it enables the distinction between major and subtle motions.

Capacitive pressure sensors have been intensively investigated because of their high sensitivity to monitor static pressure and low hysteresis compared to other pressure sensors based on piezo resistivity. The capability of developing sensitive wearable sensors with high performance and flexibility in direct contact to human skin has been proven. The sensing performance of capacitive pressure sensors can be defined by the change of capacitance $\Delta C/C_o$ in response to applied pressure P as $S=\Delta C/C_o \times 1/P$. The following sections discuss the recent advances in the development of capacitive-type strain and pressure sensors for wearable applications.

### 3.1 Stretchable capacitive-type strain sensors

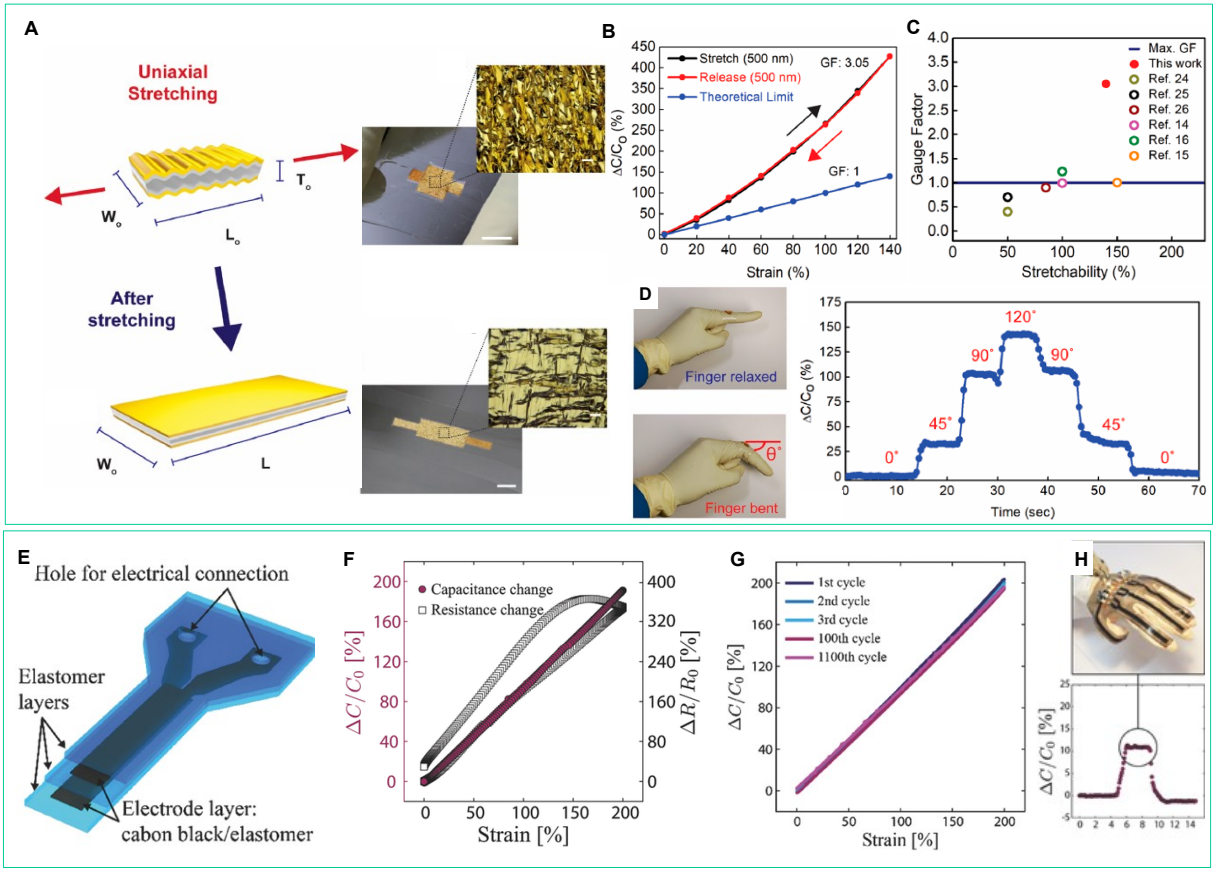


**Figure 7**. Stretchable capacitive-type strain sensors. (A) Wrinkled capacitive structure enables high stretchability under uniaxial strain. (B) Au film strain sensors under stretching. (C) Capacitance change under strain with a GF of up to 3.05. (D) Graph showing the sensitivity of capacitive strain sensors compared to the literature, indicating the limited GF of around 1. [46]

Copyright 2018, American Chemical Society. (E) Carbon black/elastomer capacitive and resistive strain sensors. (F) Capacitive-type strain sensors have a low hysteresis compared with resistive ones. (G) Repeatability of the capacitance-strain curve under multiple loading cycles. (H) Application of the capacitive-type strain sensors for wearable applications. [49] Copyright 2019, Wiley-VCH.

Capacitive strain sensors can convert mechanical deformation (stress/strain) into the change of sensor capacitance. High sensitivity of capacitive sensors is desirable to distinguish large and subtle deformations. The capacitive-type strain sensors that used a parallel capacitor have a limitation of strain sensitivity with a maximum theoretical gauge factor of 1, which is much lower than that of strain sensors employing a resistive-type principle. However, capacitive strain sensors are suitable for a wide range of practical applications owing to their linear response to applied strain. Under application of uniaxial tensile strain, the change in both thickness and area of the dielectric layer enables a linear change of capacitance to applied strain. A number of studies have successfully demonstrated capacitive strain sensors using silicone elastomer as stretchable dielectrics with a GF of around 0.3-1, linearity of 0.98-1 and stretchability of 0-500% (Table 1). **Figure 7**A shows a smart design of wrinkled capacitor structures [46] for gold electrodes that can enhance the GF up to 3 times (e.g. GF of up to 3.05 for a strain of up to 140%, Figure 7B. Figure 7C illustrates the GF value of around 1 for recent reports on stretchable capacitive strain sensors. Apart from the sensitivity, the linearity of capacitive sensors is also important for practical applications. Shintake et. al. developed a parallel plate-based capacitive strain sensor using carbon black/elastomer (Figure 7C) and demonstrated the highly linear change of capacitance with increasing strain (Figure 7F,G). The linearity (R2) of capacitive sensors was from 98% to 100% while the resistive strain sensors suffered high hysteresis (Figure 7F). Due to their high stretchability, capacitive strain sensors have also been of interest for wearable applications, including detection of human motion

(Figure 7H). Nesser et al. [114] designed gold nanoparticles between interdigitated electrodes for a capacitive strain sensor working in a 0-1.5% strain range. This sensor exhibited a maximum GF of 5 and the GF increases with increasing nanoparticle size due to the different variation of the distance between electrodes.

**Table 3**. Sensing performance of capacitive stretchable sensors based on recent advances in materials and designed structures

| Sensor | Materials & structures | Sensitivity | Pressure range | Linearity R2 | Cycles | Ref. |
|---|---|---|---|---|---|---|
| Strain | Wrinkled Au film | 3.05 | 0%-140% | 0.98 | 1000 | [46] |
| | Planar capacitor with carbon black composite | 0.83–0.98 | 50%-500% | 0.98 -1 | 10000 | [49] |
| | Multicore–Shell fiber | 0.348 ± 0.11 | 0%-250% | - | - | [115] |
| | AuNPs/ Au electrodes | 5 | 0%-1.5% | - | - | [114] |
| | Conductive knit fabric/ silicone elastomer | 1.23 | 0%-100% | 0.999 | 1000 | [116] |
| | AgNWs electrodes | −1.57 to -2 | 0%-30% | 0.9968 | 1000 | [117] |
| | Silver buckled surfaces | 0.9 | 0%-80% | 0.9982 | - | [118] |
| | Planar electrodes (hydrogels/Ag nanofibers) | 165 | 0%-1000% | Non linear | - | [119] |
| | Capacitor MXene /PVA | 0.4 | 0%-200% | 0.999 | 10000 | [120] |
| | AgNWs / Ecoflex | 0.99 | 0%-150% | - | 1000 | [121] |
| Pressure | Pyramidal capacitive PDMS structures | 2.5 $kPa^{-1}$ | 0-600 kPa (0%-15%) | - | 2000 | [45] |
| | Microridge- air cavities | 0.03-0.15$kPa^{-1}$ | 0-10 kPa | - | 5000 | [122] |

| | | | | | |
|---|---|---|---|---|---|
| AgNW-PMMA wrinkle | 2.76 $kPa^{-1}$ | 0-1 kPa (0%-20%) | - | 3000 | [123] |
| PEDOT:PSS/g-PDMS wrinkle structures | 7 $kPa^{-1}$ | 0-10 kPa (0%-100%) | - | 10000 | [22] |
| Micropyramid structures of graphene electrodes | 3.19-7.68 $kPa^{-1}$ | 0-4 kPa | - | 1000 | [124] |
| Metal electrodes Ag NFs and Ecoflex dielectrics | $5.5\times10^{-4}$-0.01887 $kPa^{-1}$ | 0-700 kPa (0%-60%) | | 2200 | [125] |
| AgNWs electrodes and TPU dielectrics | 0.06-4.2 $kPa^{-1}$ | 0-32 kPa | - | 10000 | [126] |
| Ti/Au electrodes/PDMS wrinkles | 14.268 $kPa^{-1}$ | 0-40 kPa (0%-50%) | - | 10000 | [127] |
| AgNWs electrode and polyimide dielectric film | 0.077-1.2 $kPa^{-1}$ | 0-15 kPa | - | 10000 | [128] |
| PEDOT:PSS, Ecolfex with airs for dielectrics | 0.56% $kPa^{-1}$ 0.77% $kPa^{-1}$ | -60-0 kPa 0-20 kPa (0%-10%) | - | 1000 | [129] |
| PEDOT:PSS /PDMS/silica | Upto 1 $kPa^{-1}$ | 0-10 kPa | - | 1000 | [130] |
| Au/PET/PDMS micropillar | 0.42 $kPa^{-1}$ | 0-16 kPa | - | 1000 | [131] |
| Cu/Ni electrodes/bionic Komochi Konbu dielectric | Upto 0.17 $kPa^{-1}$ | 0-255 kPa | - | 1000 | [132] |
| CNT-Ecoflex electrodes and 3D porous dielectrics | 0.077-0.6 $kPa^{-1}$ | 0-140 kPa (0%-80%) | - | 1000 | [133] |

### 3.2 Stretchable pressure sensors

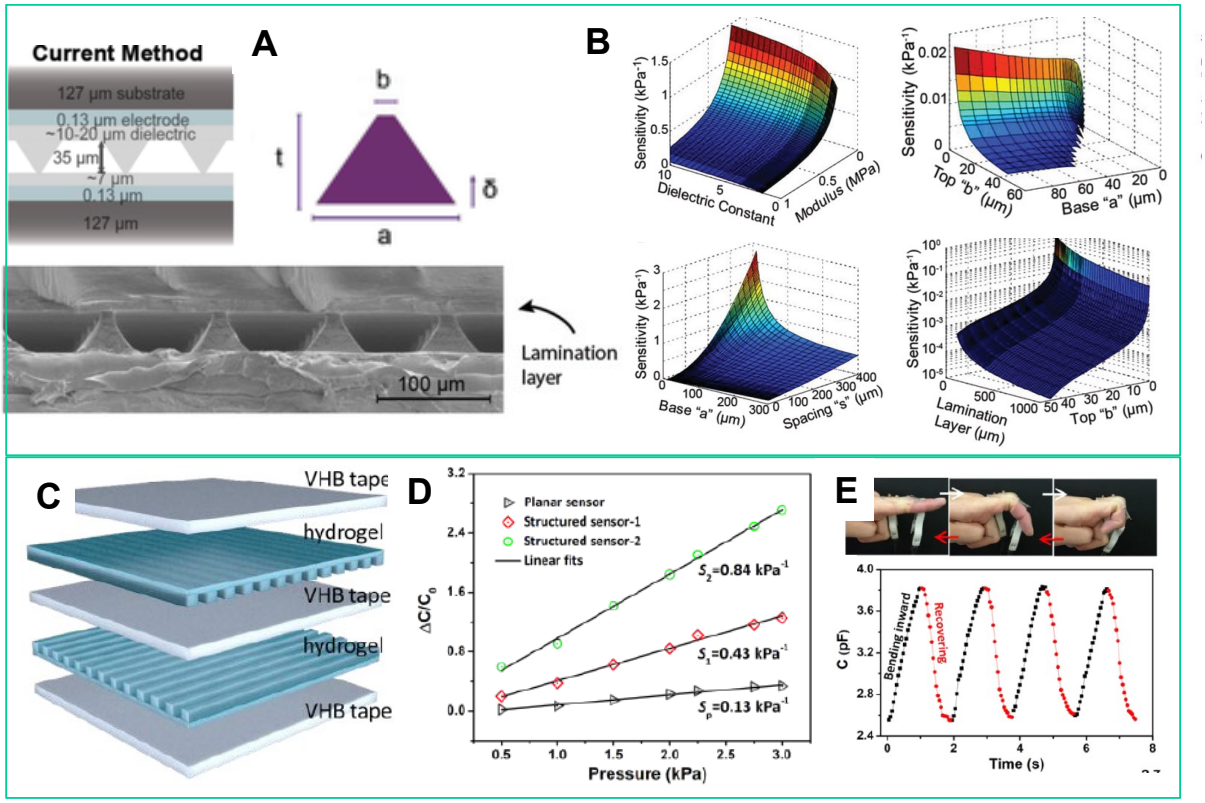


**Figure 8**. Stretchable capacitive-type pressure sensors. (A) Dielectric pyramidal structure for pressure sensing. (B) Tuneable sensitivity. [45] Copyright 2019, Wiley-VCH. (C) Parallel lines for electrodes of capacitive pressure sensors. (D) Tuneable sensitivity of capacitive pressure sensors with changing the distance between parallel lines. (E) Capture of human motion. [57] Copyright 2019, Royal Society of Chemistry.

Capacitive pressure sensors have advantages in terms of linearity, pressure sensitivity and proximity sensing. Conventional designs used parallel-plate capacitive concepts with a simple governing equation ($C \sim 1/d$ where C and d are capacitance and distance between two parallel plates, respectively). This characteristic allows the versatility of the pressure sensors for use in numerous applications to detect forces/pressures with low power consumption. The recent designs of flexible and stretchable capacitive pressure sensors use two electrodes separated by

a microstructured dielectric layer that can be deformed under applied pressure. The structural design of dielectric layers is important to control the sensing performance of such sensors. These designs include wrinkled structures [22, 123, 127], pyramid shapes [45, 134, 135], air gaps [122, 129], conformal structures [114, 120], micropillars/microtower patterns [128, 131], bionic komochi konbu structures [132], parallel lines [57], nanofibers [126], microporous structures [133], and ecoflex layers [136, 137]. The materials and designs of capacitive pressure sensors are chosen to achieve high stretchability, high sensitivity, wide pressure range, low detectable pressure limit and high linearity. The current interests focus on the controllable and structural designs of sensors for tenable sensitivity and wide pressure sensing ranges. For example, **Figure 8**A shows a rational design of a capacitive pressure sensor using a dielectric pyramidal structure for pressure sensing of biosignals [45]. The pressure sensitivity of this sensor can be tuneable by changing the size of the pyramid and dielectric properties of the material (Figure 8B). Figure 8C shows the design of parallel lines for electrodes, and dielectric layer (VHB tape) [57]. The sensors with larger spacing between lines have a higher sensitivity compared to flat electrodes and small spacing lines (Figure 8D). This sensor has been demonstrated for smart electronics, artificial intelligence, and motion capture (Figure 8E).

**4. Integrated capacitance and inductance in wireless technology for wearable sensors**

As aforementioned, electromechanical sensors utilize the change of resistance, capacitance and inductance to evaluate the mechanical stimuli. The increasing demand on the portability, comfortability and compactness of stretchable sensors has added great interest to the development of wireless technology by integrating capacitance and inductance into a stretchable platform. Wireless technology such as near field and radio frequency communications has offered an advanced platform for detection of physical signals, including strain, pressure and temperature from the human body. Wireless wearable sensors have typically employed passive electronic components, including a capacitor and inductor to form a resonance circuit and transform the physical signals via electromagnetic fields. The change

of capacitance or inductance in this resonance circuit will lead to the shift of the resonant frequency that qualifies the amplitude of the physical inputs. This technology has certain advantages in terms of simplicity in implementation and no power source required. The coupling of inductance and capacitance at resonance frequency is used to evaluate the change in mechanical signals (e.g. pressure and strain). This coupling with a design of near zero resistance will be suitable for applications towards zero-power consumption.

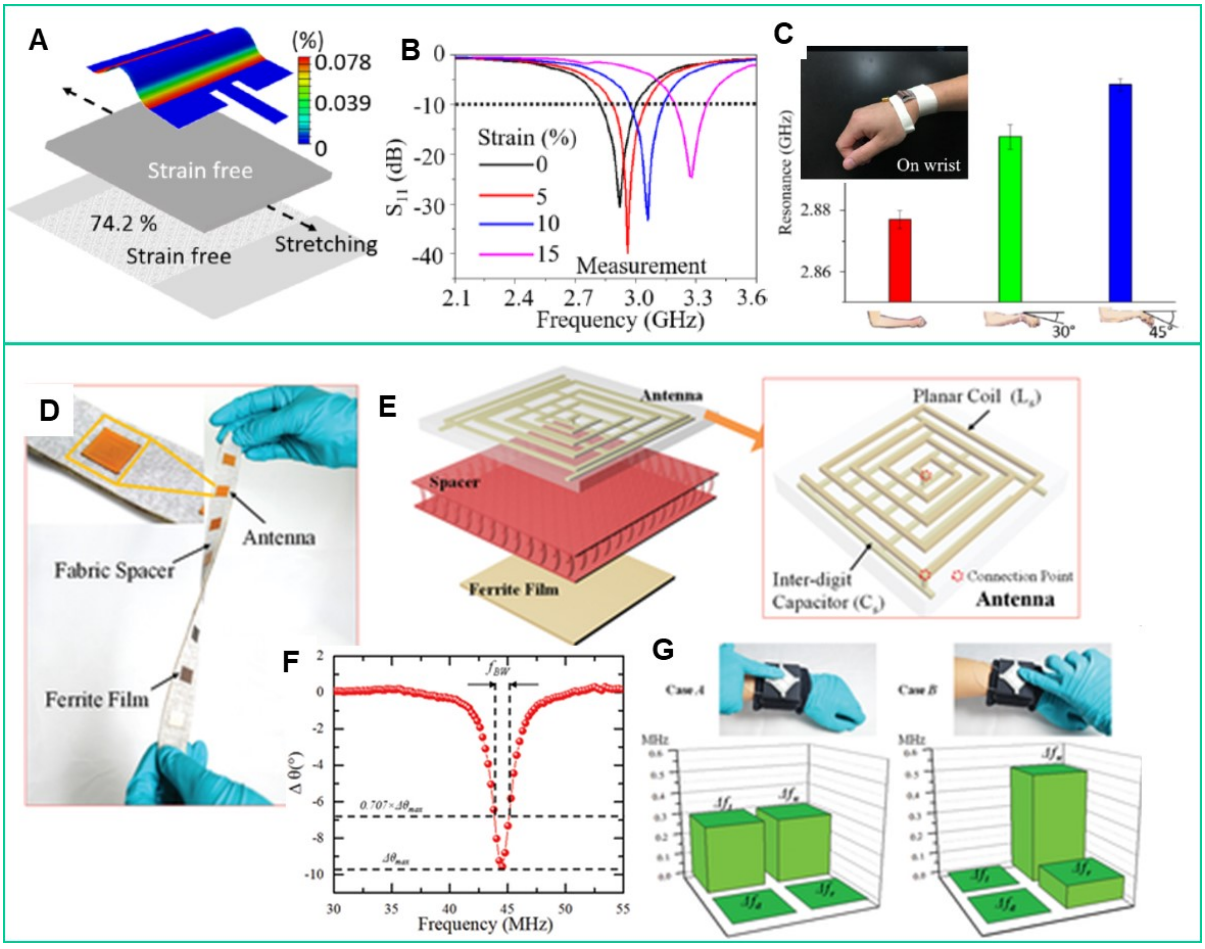


**Figure 9**. Resonance-based wearable sensors. (A) Structural design of stretchable antennas for strain sensing. (B) Resonance frequency shift with applied strain. (C) Application of stretchable antennas for human motion detection. [27] Copyright 2019, American Chemical Society. (D) A textile-based wireless pressure sensor array (WiPSA). (E) Structure of WiPSA. (F) Phase

change of the WiPSA. (G) WiPSA for wearable applications as smart wristband. [138] Copyright 2019, Willey-VCH.

Wireless technology, including antennas, has been used as an effective method of communication for large volumes of data. This has extended to applications in strain and pressure sensing. For example, there has been tremendous progress in the development of radio frequency antennas for stretchable mechanical sensors. Recent studies have focused on the structural design of antennas to achieve high flexibility, stretchability and sensitivity towards applications in strain sensing and detecting of human motion. For example, Zhu et. al. [27] employed wavy structures (**Figure 9**A) for stretchable antennas having stable radiation properties and sensitivity enhancement of 1.49-fold to 3.35-fold compared to AgNWs [139] and liquid metal [140] micro antennas. Figure 9B shows the shift of the resonant frequency corresponding to the applied strain (0-15%). The application of antennas for wearable applications has also been successfully demonstrated (Figure 9C). The recent development of E-textile technology also offers an advanced design of flexible porous textile structures. For example, the deformability of fabric spacer can tune the distance from a ferrite film to an inductor, leading to changes in the inductance or resonant frequency of the LC antenna [138]. Figures 9 D and E illustrate the structure of a textile-based wireless pressure sensor array (WiPSA). The resonant frequency defined from the phase change is the indicator for the strain sensing (Figure 9F). Figure 9G shows the remote tactile sensing application of the WiPSA in an example of an integrated smart wristband.

## 5. Materials for stretchable mechanical sensors

The development of advanced materials is one of the driving forces for tremendous progress on the performance enhancement of stretchable electromechanical sensors for wearable applications. In this section, we will discuss the wide range of materials used to develop electromechanical sensors, including intrinsic stretchable materials (e.g. ionic liquids, liquid

metals and conductive polymers), nanomaterials (e.g. nanoparticles, metal nanowires, carbon nanotubes and 2-dimentional (2-D) materials), nanocomposites of conductive nanomaterials/fillers and stretchable nonconductive matrix, and new materials for ultra-high performance and toward new applications.

**5.1 Intrinsic stretchable conductor**

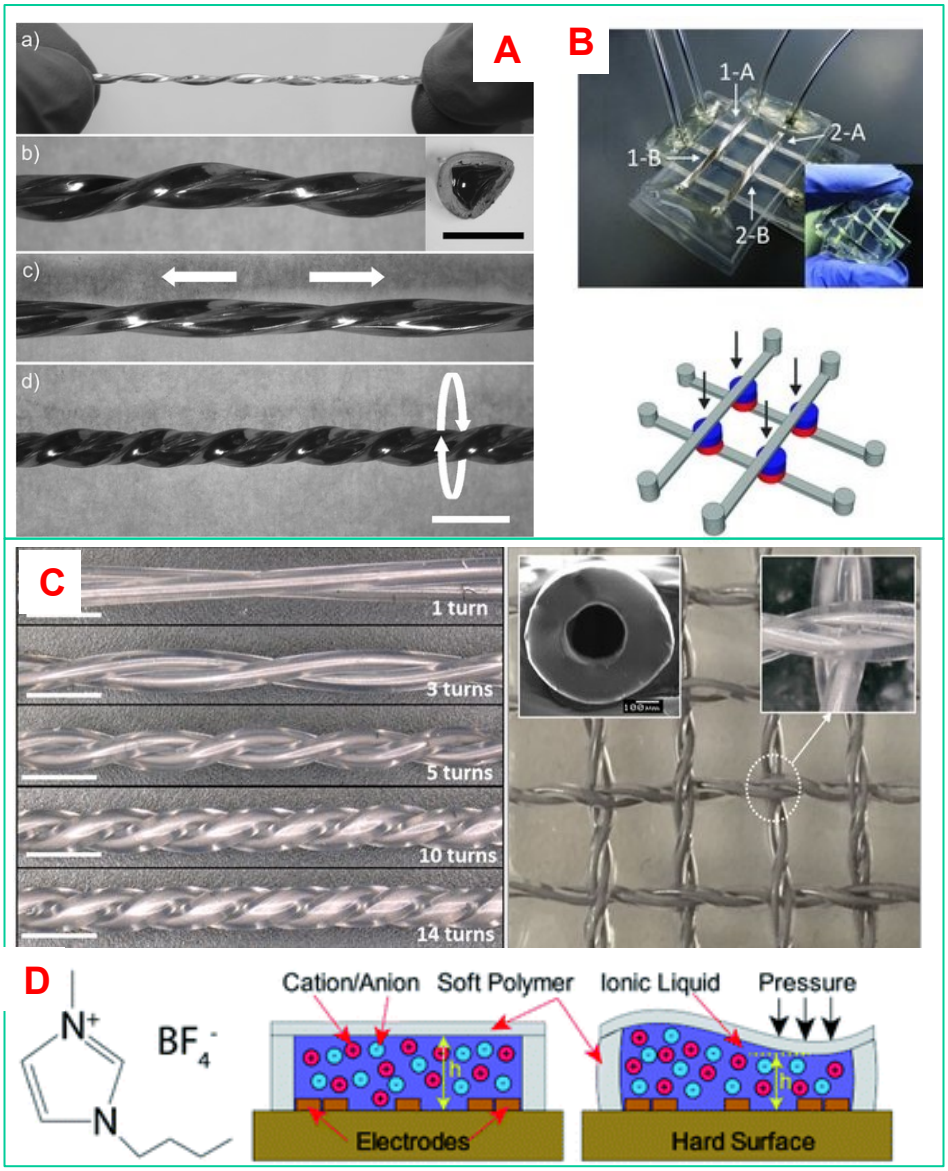

**Figure 10**. Ionic liquid and liquid metals for stretchable mechanical sensors. (A) Stretchable capacitive strain/touch sensors utilising core-shell liquid metal fibers. (B) Crossbar array of memristor using EGaIn liquid metals. [55, 141] Copyright 2017 & 2011, Wiley-VCH. (C) Woven electronic sensing fabric using twisted conductive microtubules. Printed with permission from Nature 2017 [142]. (D) Repopulation of cation/anion in a pressure sensor using ionic liquid [BMIM]+[BF4]-. [143] Copyright 2019, Royal Society of Chemistry.

**Liquid metals** such as eutectic gallium-indium alloy (EGaIn) and gallium−indium−tin (GaInSn) typically exist in the form of liquid at room temperature. These liquid metals have low toxicity, low melting points of -19ºC to 15.5ºC and high conductivity of $3.5\times10^6$ $Sm^{-1}$ [144, 145]. Liquid metals have unlimited deformability and high suitability for developing stretchable devices [61, 146]. The mechanical and sensing properties of electrodes for stretchable sensors using liquid metals are governed by the elastomeric substrates and containers, including PDMS and ecoflex [54, 55, 144]. This characteristic led to the development of highly stretchable sensors that can wrap around curved surfaces without damage at large dynamic mechanical changes; therefore, liquid metals embedded in elastomers can be employed to human-body motion sensing, skin for intelligent robots and stretchable keyboard interfaces [144, 147]. Apart from serving as connecting wires or electrodes [148, 149], liquid metals have been deployed as strain and pressure sensors using the change in inductance, capacitance or a combination of both in a stretchable antenna that tunes the resonance frequency [150-152]. For example, **Figure 10**A shows the example of a stretchable capacitive pressure sensor using LM EGaIn incorporated into a hollow elastomeric capillary core-shell structure [55]. LMs have been utilised for developing pressure sensors for meristors (Figure 10B). The main challenges of processing liquid metals are caused by their limited capability of flowing [153]. Embedding LM into elastomer fibres or printing of LM have been employed to fabricate stretchable sensors [146, 154]. Miniaturisation of stretchable sensors with high resolution (below 5 um) has been

successfully demonstrated using lithography, wettability regulation and laser ablation [59, 155-157]. More flexible/stretchable electronics and sensors employing liquid metals have recently been reviewed in detail [144].

**Ionic liquids** are known as molten salts that are electrically conductive owing to the conduction of ions [158]. Ionic liquids and gels have a high stretchability (typically above 600%) due to their low Young's modulus [68, 159]. The mechanical stress/strain deforms the container while the volume of ionic liquids remains unchanged. The sensing mechanism of ionic liquid is attributed to the relocation of cation and anion or the repopulation of the conductive ions [143]. Therefore, the sensitivity of strain/pressure sensors based on ionic liquids/gels is relatively low under a large stretchable range of strain [39, 143]. These materials are typically designed in the architecture of resistors or capacitors towards strain sensing and touch applications [160, 161]. For example, Figure 10C shows the core-shell structure of ionic liquid embedded in carbon fibre rods for strain sensing and wearable applications [142]. The deformability of ILs inside containers has been used for multi-touch and pressure sensing towards artificial and intelligent human-machine interfaces (Figure 10D) [143]. The main challenges for stretchable ionic mechanical sensors are to form reliable bonding with its container materials, including elastomers [57, 68]. **Table 4** summarises the properties of some common intrinsic materials used for electromechanical sensors.

**Table 4**. Properties of intrinsic stretchable materials for electromechanical sensors

| Materials | Conductivity ($10^{-3}$Scm$^{-1}$) | Stretchability (%) | Young's modulus (kPa) | Transparency (%) |
|---|---|---|---|---|
| Ionic liquids/gels | 1 | >600 | 10-100 (gels) | ~100 |

| | | | | |
|---|---|---|---|---|
| Liquid metals | $10^4$ | >800 | - | - |
| Conductive polymer | 4100<br>0.05 | <5%<br>100% | 2GPa<br>- | -<br>- |

### 5.2 Conductive polymer

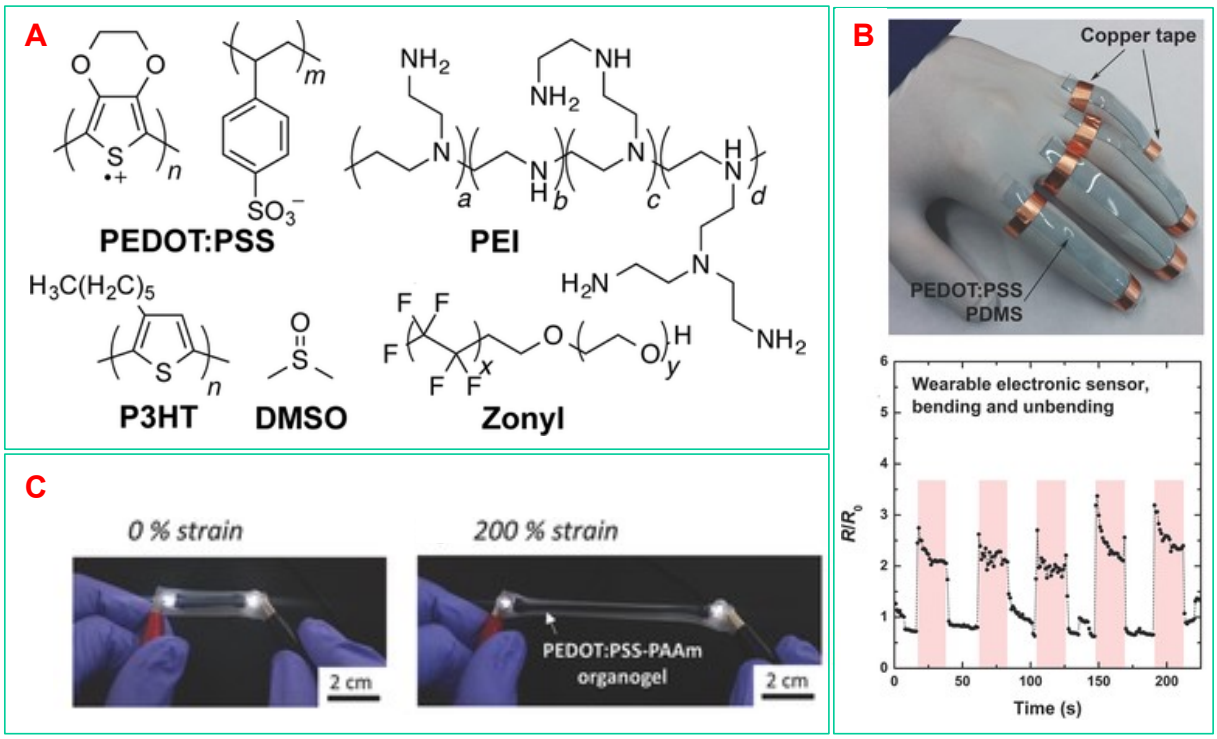


**Figure 11**. Poly(2,3-dihydrothieno-1,4-dioxin)–poly(styrenesulfonate) (PEDOT:PSS) for stretchable sensors. (A) Chemical structures of PEDOT:PSS, PEI, P3HT, DMSO, and Zonyl. (B) Application of PEDOT:PSS for human motion detection. [162] Copyright 2015, Willey-VCH. (C) Blending PEDOT:PSS-PAAm orgenogel with stretchability and conductivity. [40] Copyright 2016, Willey-VCH.

Currently, stretchable mechanical sensors have used conductive polymer thanks to its nature of flexibility, stretchability and high conductivity. The high conductivity comes from the transport

nature of combining ionic and electron conductions that lower the impedance of the materials. The most common conductive polymer is poly(2,3-dihydrothieno-1,4-dioxin)–poly(styrenesulfonate) (PEDOT:PSS) that has attracted great interest for physical and stretchable mechanical sensors [163]. PEDOT:PSS has a limited deformability nature of 5% as it has a relatively large Young's modulus of 2 GPa consisting of semicrystalline conjugated PEDOT polymer doped with acidic PSS. The main challenges of using PEDOT:PSS for stretchable sensors are its expansion of the stretchability. Effort has been given to incorporating PEDOT:PSS with other materials to achieve both high conductivity and stretchability. One of the common methods is to use co-solvents [164], nonionic surfactants (e.g. Zonyl FS-300 and Triton-X) and ionic salts [162, 165-167]. For example, dimethylsulfoxide (DMSO) was incorporated with PEDOT:PSS to increase conductivity [168] and polyethyleneimine (PEI) was laminated to PEDOT:PSS to enhance its tensile modulus and ductility [164]. This method expands the stretchability of PEDOT:PSS to 80% while the conductivity is kept high and stable. **Figure 11**A shows the chemical structures of PEDOT:PSS and incorporating materials [162]. The application of PEDOT:PSS for human motion detection has also been demonstrated (Figure 11B) [162]. The mixture of PEDOT:PSS/Acrylamide Organogels could be used for wearable sensors with stretchability of upto 200% (Figure 11C). Another approach is to blend PEDOT:PSS with high-molecular-weight polymers including poly(poly(ethylene glycol)methyl ether acrylate) and poly(vinyl alcohol) [169, 170]. However, the stretchability and conductivity are lower than these reported using nonionic surfactants.

### 5.3 Nanocomposite

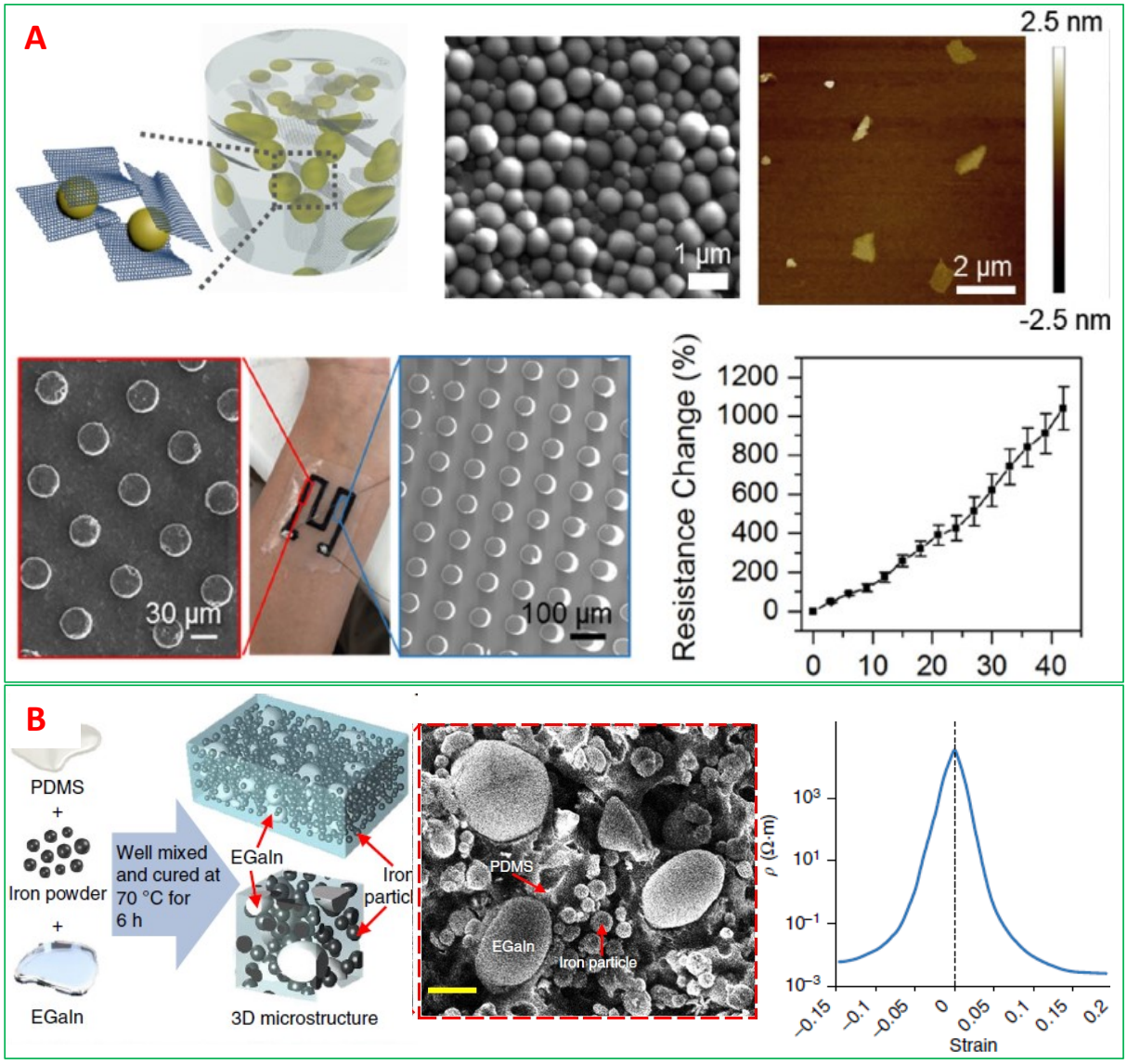


**Figure 12**: Nanocomposite stretchable strain sensors. (A) Stretchable strain sensors using a versatile PDMS submicrobead/graphene oxide nanocomposite ink. [36] Copyright 2019, Elsevier (B) Liquid metal-filled elastomer composite for strain sensor with positive piezoconductivity. [171] Copyright 2019, Nature Publishing Group.

Stretchable nanocomposites are typically the formation of a stretchable composite of an electrically conductive material (e.g. AgNWs, CuNWs, CNT and graphene) and nonconductive stretchable material (e.g. PDMS) [172, 173]. The conductivity and mechanism of nanocomposites are based on the percolation network of conductive fillers in the stretchable

matrix [174]. However, the conductive fillers have typically poor stretchability. For example, PEDOT:PSS and graphene have a typical limited stretchability of 5% and 7%, respectively [175, 176]. Therefore, these nanomaterials are embedded to form composite materials with high stretchability and high sensitivity to mechanical deformation [54]. In terms of functionalities, the network of conductive fillers provides electrical conduction for sensing, and polymer matrix supports desirable mechanical properties for stretchable devices [36].

The desirable properties of polymer matrices include mechanical stretchability, thermal stability, ease of production, and high adhesive capability. The common polymer materials for stretchable mechanical sensors are PDMS [177], polyimide (PI) [178], polyethylene terephthalate (PET) [179], ecoflex [180], and paper [181]. Among these, PDMS is the most used material for such sensors due to its additional advantages of low Young's modulus (0.4-3.5 MPa), low cost, transparency, low autofluorescence, good moldability and versatility [2, 36].

*5.3.1 Carbon nanomaterials and nanocomposites*

One-dimensional (1-D) carbon nanotube (CNT) has been known as a suitable conductive filler for stretchable mechanical sensors due to its high conductivity. Intrinsic CNT nanofibers, including yarns and highly oriented films, have been deployed for strain sensing with relatively low sensitivity (GF<1) and low stretchability of up to 5% [182,183]. CNT fibers showed the ease of forming dispersed solution in proper solvents and high aspect ratio to form the percolation in the composite. For example, CNT/PDMS composites have been utilised for wearable strain sensors with a high gauge factor of up to $10^7$ [184] and a stretchability of up to 300% [2]. Two-dimensional (2-D) graphene and reduced graphene oxide (rGO) with excellent electrical and optical properties have been constructed on PDMS substrates to develop strain sensors. For example, the graphene–nanocellulose nanopaper embedded into PDMS has been successfully demonstrated for stretchable strain sensors (up to 100% strain and GF of 4) [185]. The challenge of blending graphene and PDMS is to form high viscosity inks while possessing

self-supporting viscoelasticity after printing. In a later work, the graphene stretchability has been improved to 50% and GF value of below 50 [36, 186, 187]. **Figure 12**A shows the PDMS submicrobead/graphene oxide nanocomposite for direct writing of stretchable strain sensors for human motion detection [36]. To further increase the sensitivity and stretchability of graphene-based composite sensors, ecoflex has been used to provide a GF value of up to 457 and stretchability of 100% strain [188].

*5.3.2 Metal nanowire, nanoparticle and its nanocomposite*

In addition to the carbon-based composites, metal composites have also attracted great interest for stretchable sensors and electronics [37,189-191]. For example, the nanocomposite of silver nanowire (AgNW) network and PDMS elastomer has been demonstrated for motion detection with a gauge factor of 2 to 14 [2,192] and pressure sensors [193]. Ag flakes and AgNPs have been embedded into elastomeric materials with high conductivity and stretchability [194-196]. These composites have a high conductivity of above 6000 $Scm^{-1}$ and stretchability of 900% strain. AgNPs and AgNWs have been employed for the development of sensitive 3D touch sensors with a design of self-generated multiscalse structures [197]. Copper nanowire (CuNW) and its nanocomposites have been also used to develop flexible capacitive-force touch sensors and wearable electronics [198,199].

Metal nanowires and their composites have also attracted considerable interests toward high performance transparent sensors and electronics, due to their operational capability while maintaining significant transparency [189,191,192,197,198,200,201]. Stretchable transparent sensors are suitable for wearable applications as they offer high sensitivity and comfortable wearing while avoiding inconvenience during daily activities. The transparency and performance of such sensors depend on the density of the percolation network of metal nanowires. Using AgNWs percolation networks will enable the maintenance of consistent performance under large deformation and avoid leaking issues in other stretchable transparent sensors such as microfluidic strain sensors [202].

### *5.3.3 Composite of conductive polymers*

Some interest has been shown in developing stretchable mechanical sensors using composites of conductive polymers and nonconductive polymers. These composites have advantages of simplicity in preparation and strong adhesion to the polymers. However, the conductivity of this composite is typically much lower than that of metal-based and carbon-based stretchable sensors. As discussed in the previous section, PEDOT:PSS blended on PU and other elastomers is of interest for mechanical sensing in wearable applications due to its excellent stretchability and high sensitivity. Some other mixtures of PEDOT:PSS and polyvinyl alcohol (PVA) have shown a high resistivity ($6\times10^4$-$2\times10^7$ Ωcm) and high sensitivity (GF value up to 400) but low stretchability (<5% strain) [203, 204].

### *5.3.4 Other nanocomposites*

Most composite strain sensors have an increase in electrical resistance with increasing tensile strain due to the increase in tunneling distance [173, 205, 206] and crack propagation [43, 207, 208]. However, these composites are more resistive with higher train or deformation, leading to the limited range of sensing capability and other undesirable characteristics. Therefore, recent research focuses on the development of liquid metal nanocomposites that have negative piezoresistance. Under tensile stretching, the liquid metal droplets of the nanocomposite can flow out and create new pathways connected with adjacent solid conductive fillers, resulting in a decrease of electrical resistance. For example, Figure 12B shows the formation of the hybrid/composite of liquid metal microdroplets, metallic magnetic microparticles composed of carbonyl iron (Fe) and PDMS [171]. This composite exhibited a large negative piezoresistance due to the squeezing of the Fe particles surrounding the PDMS and liquid metal microdroplets, leading to the decrease of PDMS thickness and direct contact of the Fe particles and liquid metal microdroplets [171].

### 5.4 Ceramic materials and designs toward harsh environment applications

There is an emerging demand for flexible and stretchable electromechanical sensors and electronics working in harsh environments. Ceramic materials including silicon carbide have proven to show excellent properties for electronics and sensors owing to their chemical inertness and capability to work reliably at high temperatures. Recent advances in the development of ceramic materials with a focus on two-dimentional (2D) metal carbide and SiC are discussed in this section.

#### *5.4.1 Two-dimensional (2D) metal carbides*

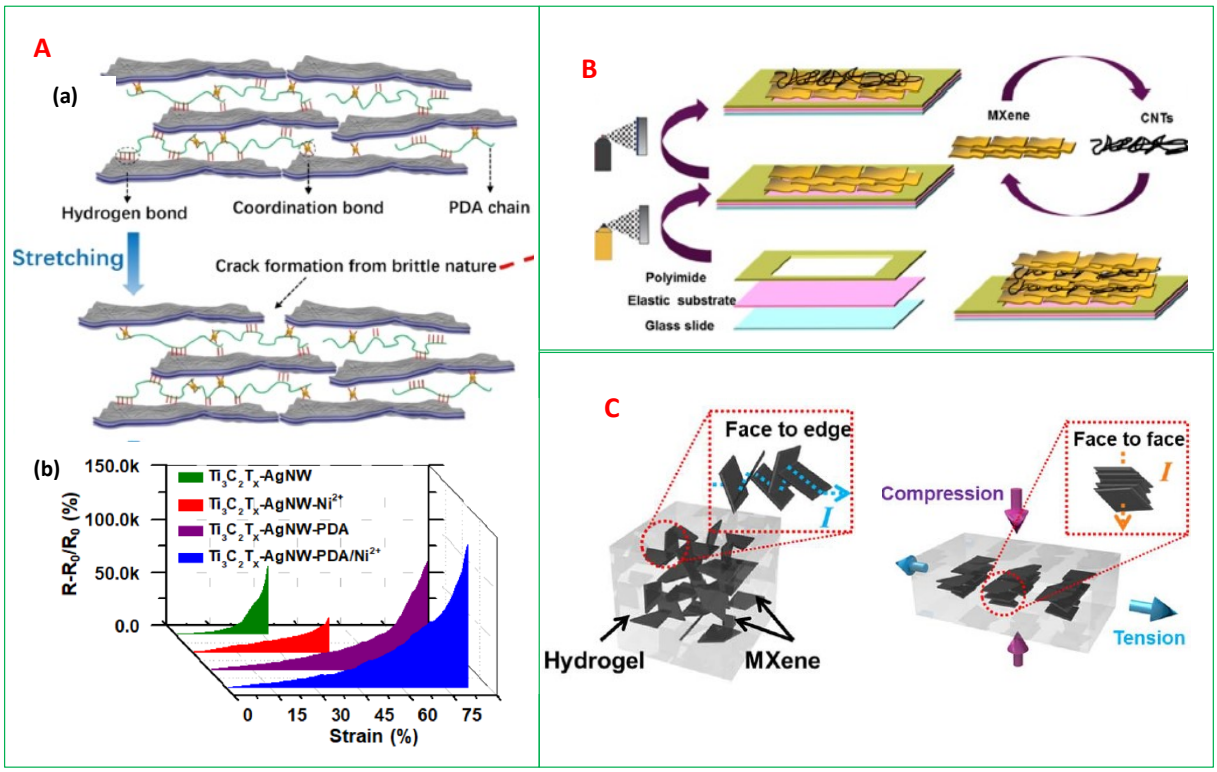


**Figure 13**: MXene and its composites for mechanical sensing applications. (A) Hierarchical layered structures of MXene composite of Ti3C2Tx-AgNW-PDA/Ni2+ strain sensors with the bonding changes with stretching (top) and the resistance changes vs strain of different MXene composites (bottom). Reprinted with permission ACS 2019 [34]. (B) Structural assembly of Ti3C2Tx MXene/CNT layer mechanical sensors. Reprinted with permission ACS 2019 [209].

(C) Sensing mechanism of MXene-hydrogel for strain sensing with a stretchability of aabove 3400%. Reproduced with permission Science 2019 [35]

Two-dimensional (2D) metal carbides, referred to as MXenes, are potential materials for mechanical sensing in stretchable and wearable applications, owing to their high electrical conductivity (e.g. 105 S/m) [52]. This material has unique electrical and chemical properties including high carrier mobility for a wide range of applications. For example, the conductivity of MXenes can be altered via the distance change between the MXene layers by applying strain. To utilise this mechanism, Mxenes are typically mixed with other materials such as CNT and rGO to form nanocomposites [209] and hydrogels [35]. Pressure sensors based on MXene/rGoO aerogel has been demonstrated with a high sensitivity of 22.56 $kPa^{-1}$ with high linearity in a wide strain range and low detection limits [210]. Shi et. al. [34] has demonstrated a MXene-based strain sensor with "brick-and-mortar" structures, **Figure 13**A (top). Ti3C2Tx-AgNW "brick" was used as a conductive block while (PDA)/Ni2+ was the "mortar" to coordinate bonding and assist the stretching functionalities. This structure offered a high sensitivity of GF upto ~8,700 with a stretchability of up to 80%, shown in Figure 13A (bottom). The high sensitivity comes from the crack formation during stretching. The rational design [209] of MXene layers/flakes/sheets in sandwich structure with CNT (Figure 13B) has been employed to develop wearable strain sensors with high sensitivity (GF~772.6), high stretchability (130%) and high stability of >5000 cycles. To enhance the stretchability, hydrogel composites incorporating MXene (Ti3C2Tx) have shown exceptionally high performance with a GF of 25 and stretchability of above 3400% [35]. In addition, compressive strain reduces the face-to-face distance between MXene nanosheets which more significantly enhances the sensing performance compared to tensile strain (Figure 13C).

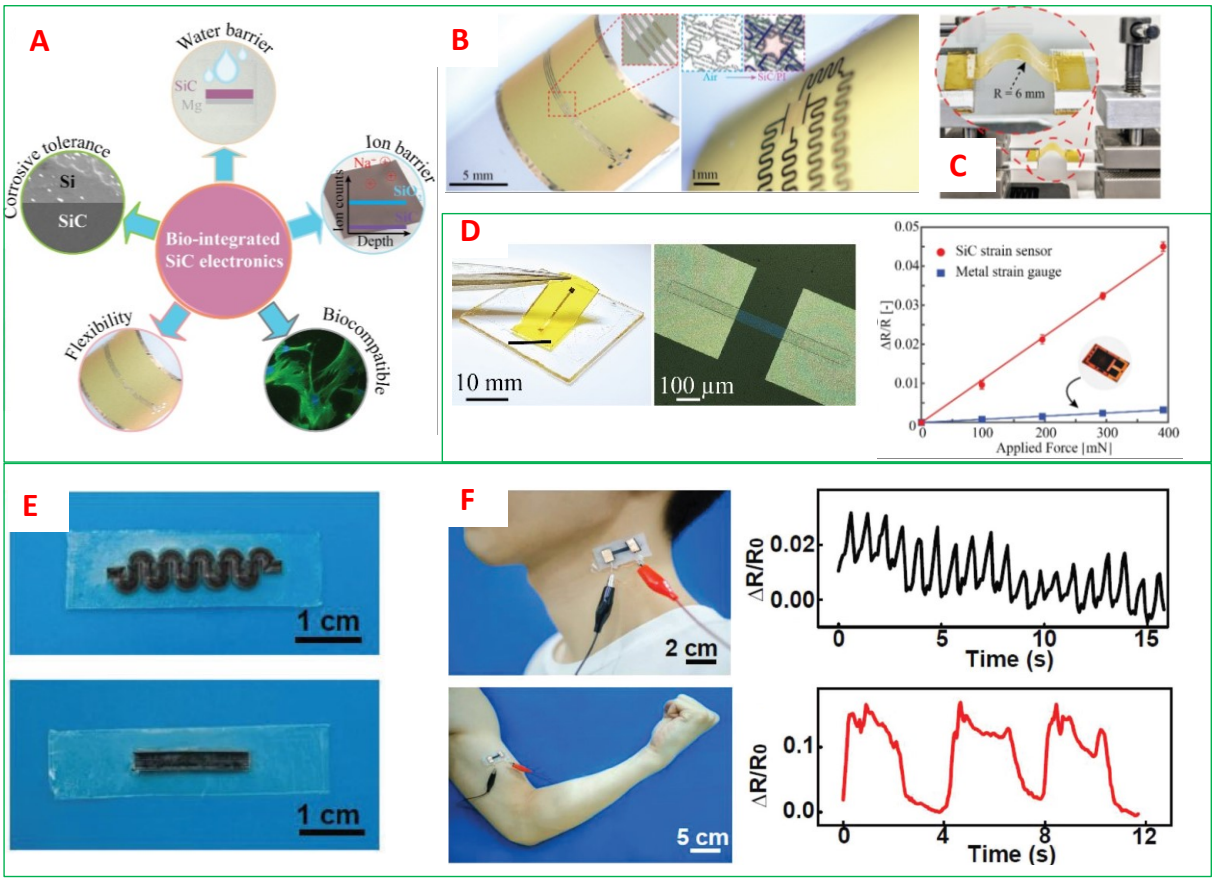


**Figure 14**: Silicon carbide (SiC) for wearable electromechanical sensors operating harsh environments. (A) SiC for flexible & stretchable electronics and sensors toward harsh environment applications. (B) SiC nanofilms transferred onto flexible PI substrates. (C) SiC flexible sensor testing. (D) SiC flexible strain gauge and its high performance compared to commercialised strain gauges. [4] Copyright 2019, American Chemical Society. (E) SiC strain sensors by laser direct writing for (F) wearable applications. [47] Copyright 2019, Willey-VCH.

### *5.4.2 Silicon carbide (SiC) for harsh environment applications*

Recently, the challenges of monitoring stress/strain in space exploration, geothermal industries and marine applications have raised increasing interests for flexible and stretchable electromechanical sensors that are able to work reliably in harsh environments. The harsh environment applications include electronic devices used in extremely low or high temperatures, high radiation, high salinity, high humidity, or any combination of these conditions [211]. The sensors should function consistently in hostile conditions including at high temperatures, high

corrosion and humidity. In some successful demonstrations, metals (e.g. nickel) and titanium alloys have shown the excellent long-term performance at high temperatures [212, 213] and in aerospace applications [214].

In addition, ceramic materials such as silicon carbide (SiC) have been proven to have excellent electromechanical properties for highly sensitive sensors operating at high temperatures [215,216] or requiring biocompatibility and implantability [4] (**Figure 14**A). However, high quality single crystalline cubic SiC materials could only be formed on Si wafers at low cost by low pressure vapour deposition (LPCVD) processes, where the SiC/Si platform is rigid and not suitable for flexible and stretchable electromechanical sensors. Therefore, transferring technologies have been developed to form SiC nanofilms embedded in flexible/stretchable substrates including polyimide (PI) [4] (Figure 14B). SiC-on-PI platform has been characterised for flexible electronics and sensors (Figure 14C). For example, Figure 14D demonstrates the flexibility of SiC-on-PI for strain gauges with excellent performance compared to commercialised strain gauges. SiC wearable strain sensors with a detection limit of 0.05% and high durability (10000 cycles) have also been formed by a direct laser writing method [47] (Figure 14D). These sensors have been successfully demonstrated for monitoring external stimuli, including e-skin application (Figure 14E). Some materials (e.g. SiC and GaN) for flexible/stretchable electronics and electromechanical sensors used in harsh environments have been developed and reviewed [211,217-219].

**6. Conclusion and outlook**

The present review highlights recent major developments of stretchable and wearable electromechanical sensors with a focus on materials and rational/structural designs toward high sensitivity and high stretchability. Intrinsic stretchable materials have been employed for wearable strain and pressure sensors with exceptionally high stretchability. The freedom in designs of electromechanical sensors is only limited by the geometry of stretchable containers/channels that cover the intrinsic materials. However, the sensitivity of these sensors

is restricted by the natural piezoresistance of the materials. On the other hand, nanomaterial-based sensors with conductive blocks embedded or distributed in polymers/elastomers have a high sensitivity but limited stretchability. The stretchability and sensitivity could be enhanced by engineering the rational structures with simple fabrication strategies, enabling the development of numerous wearable applications. The conventional materials for stretchable and wearable electromechanical sensors have limited access to environments including human bodies and harsh conditions. The investigation of these materials toward environmentally-friendly applications would be of interest in future research. The new materials for electromechanical sensors such as MXene have expanded the stretchability up to 3,400% and high sensitivity of GF over 1,000. The development of ceramic materials including metal carbide and silicon carbide would expect significant attention and process in the next few years. The interests of stretchable electromechanical sensors and electronics is emerging for bioapplications (e.g. implantable sensors) and harsh environments, including high temperatures and corrosion. New design strategies to transfer hard materials (e.g. Si and SiC) to soft substrate will enable electromechanical sensors and electronics to work reliably in a wide range of applications. In addition, the new materials have added more functionalities of the electromechanical sensors including self-healing and bio comparability. However, there are challenges to achieving both high sensing performance/sensitivity and a wide range of stretchability. Transparent materials including ionic liquids and metal nanowires would be continuingly of interests for stretchable sensors as these can enhance the comfortability of wearable devices in long term services.

Research on structural and rational designs have significantly enhanced the sensitivity and stretchability of electromechanical sensors. For example, the design of a sensing element at stress concentration areas has been employed as an effective strategy to enhance the sensitivity of stretchable strain sensors. Crack propagation is one of the most popular strategies to improve sensitivity of stretchable strain sensors while this method leads to the increase of the electrical

resistance with increasing tensile strain, limiting the applications of stretchable sensing. The design strategy is developing toward low power or zero power consumption by using highly conductive stretchable conductors. Pure-capacitance and inductance based electromechanical sensors could be suitable for the next generation of near zero-power consumption devices. The main challenges for future development of stretchable electromechanical sensors is to integrate multiple electromechanical sensing functionalities and power supply into a single technology platform. Further investigation on the development of sensing functionalities, linearities, long-term stabilities and stretchable conductors would enable the multifunctional sensing electronic devices for the next generation of wearable applications.

**Acknowledgements**
This work has been partially supported by Australian Research Council grants LP150100153 and 370 LP160101553

Received:
Revised:
Published online:

**References**

1. T. Yamada,Y. Hayamizu,Y. Yamamoto,Y. Yomogida,A. Izadi-Najafabadi,D. N. Futaba,K. Hata, *Nature nanotechnology* **2011,** *6*, 296.

2. M. Amjadi,A. Pichitpajongkit,S. Lee,S. Ryu,I. Park, *ACS nano* **2014,** *8*, 5154.

3. S. Yao,Y. Zhu, *Nanoscale* **2014,** *6*, 2345.

4. H.-P. Phan,Y. Zhong,T.-K. Nguyen,Y. Park,T. K. Dinh,E. Song,R. K. Vadivelu,M. K. Masud,J. Li,M. J. Shiddiky, *ACS nano* **2019**.

5. S. Gong,W. Schwalb,Y. Wang,Y. Chen,Y. Tang,J. Si,B. Shirinzadeh,W. Cheng, *Nature communications* **2014,** *5*, 3132.

6. S. Ryu,P. Lee,J. B. Chou,R. Xu,R. Zhao,A. J. Hart,S.-G. Kim, *ACS nano* **2015,** *9*, 5929.

7. Z. Liu,D. Qi,P. Guo,Y. Liu,B. Zhu,H. Yang,Y. Liu,B. Li,C. Zhang,J. Yu, *Advanced Materials* **2015,** *27*, 6230.

8. T. Q. Trung,N. E. Lee, *Advanced Materials* **2017,** *29*, 1603167.

9. Y. Zang,F. Zhang,C.-a. Di,D. Zhu, *Materials Horizons* **2015,** *2*, 140.

10. D. Son,Z. Bao, *ACS nano* **2018,** *12*, 11731.

11. W. A. D. M. Jayathilaka,K. Qi,Y. Qin,A. Chinnappan,W. Serrano-García,C. Baskar,H. Wang,J. He,S. Cui,S. W. Thomas, *Advanced Materials* **2019,** *31*, 1805921.

12. N. Matsuhisa,X. Chen,Z. Bao,T. Someya, *Chemical Society Reviews* **2019,** *48*, 2946.

13. S. Chen,Y. Wei,S. Wei,Y. Lin,L. Liu, *ACS applied materials & interfaces* **2016,** *8*, 25563.

14. S. Zhao,J. Li,D. Cao,G. Zhang,J. Li,K. Li,Y. Yang,W. Wang,Y. Jin,R. Sun, *ACS applied materials & interfaces* **2017,** *9*, 12147.

15. T. Yang,W. Wang,H. Zhang,X. Li,J. Shi,Y. He,Q.-s. Zheng,Z. Li,H. Zhu, *ACS nano* **2015,** *9*, 10867.

16. Z. Yi,Y. Wan,M. Qin,Q.-A. Huang, *Journal of Microelectromechanical Systems* **2019,** *28*, 321.

17. Z. Xie,R. Avila,Y. Huang,J. A. Rogers, *Advanced Materials* **2019**, 1902767.

18. Z. Xue,H. Song,J. A. Rogers,Y. Zhang,Y. Huang, *Advanced Materials* **2019**, 1902254.

19. S. Wang,Y. Huang,J. A. Rogers, *IEEE Transactions on Components, Packaging and Manufacturing Technology* **2015,** *5*, 1201.

20. S. Xu,Y. Zhang,J. Cho,J. Lee,X. Huang,L. Jia,J. A. Fan,Y. Su,J. Su,H. Zhang, *Nature communications* **2013,** *4*, 1543.

21. Y. Zhang,H. Fu,Y. Su,S. Xu,H. Cheng,J. A. Fan,K.-C. Hwang,J. A. Rogers,Y. Huang, *Acta Materialia* **2013,** *61*, 7816.

22. G. Li,Z. Qiu,Y. Wang,Y. Hong,Y. Wan,J. Zhang,J. Yang,Z. Wu,W. Hong,C. F. Guo, *ACS applied materials & interfaces* **2019,** *11*, 10373.

23. J. L. Blackburn,T. M. Barnes,M. C. Beard,Y.-H. Kim,R. C. Tenent,T. J. McDonald,B. To,T. J. Coutts,M. J. Heben, *Acs Nano* **2008,** *2*, 1266.

24. E. Roh,B.-U. Hwang,D. Kim,B.-Y. Kim,N.-E. Lee, *ACS nano* **2015,** *9*, 6252.

25. Y. Tang,Z. Zhao,H. Hu,Y. Liu,X. Wang,S. Zhou,J. Qiu, *ACS applied materials & interfaces* **2015,** *7*, 27432.

26. G. Yin,N. Hu,Y. Karube,Y. Liu,Y. Li,H. Fukunaga, *Journal of composite materials* **2011,** *45*, 1315.

27. J. Zhu,J. J. Fox,N. Yi,H. Cheng, *ACS applied materials & interfaces* **2019,** *11*, 8867.

28. X. Liu,C. Tang,X. Du,S. Xiong,S. Xi,Y. Liu,X. Shen,Q. Zheng,Z. Wang,Y. Wu, *Materials Horizons* **2017,** *4*, 477.

29. Y. Huang,W. Dong,T. Huang,Y. Wang,L. Xiao,Y. Su,Z. Yin, *Sensors and Actuators A: Physical* **2015,** *224*, 36.

30. M. R. Ramli,S. Ibrahim,Z. Ahmad,I. S. Z. Abidin,M. F. Ain, *ACS applied materials & interfaces* **2019,** *11*, 28033.

31. X. Wang,Z. Liu,T. Zhang, *Small* **2017,** *13*, 1602790.

32. Z. Lou,L. Wang,G. Shen, *Advanced Materials Technologies* **2018,** *3*, 1800444.

33. Y. Wan,Y. Wang,C. F. Guo, *Materials Today Physics* **2017,** *1*, 61.

34. X. Shi,H. Wang,X. Xie,Q. Xue,J. Zhang,S. Kang,C. Wang,J. Liang,Y. Chen, *ACS nano* **2018,** *13*, 649.

35. Y.-Z. Zhang,K. H. Lee,D. H. Anjum,R. Sougrat,Q. Jiang,H. Kim,H. N. Alshareef, *Science advances* **2018,** *4*, eaat0098.

36. G. Shi,S. E. Lowe,A. J. Teo,T. K. Dinh,S. H. Tan,J. Qin,Y. Zhang,Y. L. Zhong,H. Zhao, *Applied Materials Today* **2019,** *16*, 482.

37. P. Won,J. J. Park,T. Lee,I. Ha,S. Han,M. Choi,J. Lee,S. Hong,K.-J. Cho,S. H. Ko, *Nano letters* **2019,** *19*, 6087.

38. Y. Gao,H. Ota,E. W. Schaler,K. Chen,A. Zhao,W. Gao,H. M. Fahad,Y. Leng,A. Zheng,F. Xiong, *Advanced Materials* **2017,** *29*, 1701985.

39. D. Y. Choi,M. H. Kim,Y. S. Oh,S.-H. Jung,J. H. Jung,H. J. Sung,H. W. Lee,H. M. Lee, *ACS applied materials & interfaces* **2017,** *9*, 1770.

40. Y. Y. Lee,H. Y. Kang,S. H. Gwon,G. M. Choi,S. M. Lim,J. Y. Sun,Y. C. Joo, *Advanced materials* **2016,** *28*, 1636.

41. B. Yin,X. Liu,H. Gao,T. Fu,J. Yao, *Nature communications* **2018,** *9*, 5161.

42. J. Lee,S. Pyo,D. S. Kwon,E. Jo,W. Kim,J. Kim, *Small* **2019**, 1805120.

43. S. Pan,Z. Liu,M. Wang,Y. Jiang,Y. Luo,C. Wan,D. Qi,C. Wang,X. Ge,X. Chen, *Advanced Materials* **2019**, 1903130.

44. J. Lee,S. Shin,S. Lee,J. Song,S. Kang,H. Han,S. Kim,S. Kim,J. Seo,D. Kim, *ACS nano* **2018,** *12*, 4259.

45. S. R. A. Ruth,L. Beker,H. Tran,V. R. Feig,N. Matsuhisa,Z. Bao, *Advanced Functional Materials* **2019**, 1903100.

46. R. Nur,N. Matsuhisa,Z. Jiang,M. O. G. Nayeem,T. Yokota,T. Someya, *Nano letters* **2018,** *18*, 5610.

47. Y. Gao,Q. Li,R. Wu,J. Sha,Y. Lu,F. Xuan, *Advanced Functional Materials* **2019,** *29*, 1806786.

48. Z. Liu,D. Qi,G. Hu,H. Wang,Y. Jiang,G. Chen,Y. Luo,X. J. Loh,B. Liedberg,X. Chen, *Advanced materials* **2018,** *30*, 1704229.

49. J. Shintake,E. Piskarev,S. H. Jeong,D. Floreano, *Advanced Materials Technologies* **2018,** *3*, 1700284.

50. Y. Lee,J. Park,S. Cho,Y.-E. Shin,H. Lee,J. Kim,J. Myoung,S. Cho,S. Kang,C. Baig, *ACS nano* **2018,** *12*, 4045.

51. D. Kang,P. V. Pikhitsa,Y. W. Choi,C. Lee,S. S. Shin,L. Piao,B. Park,K.-Y. Suh,T.-i. Kim,M. Choi, *Nature* **2014,** *516*, 222.

52. H. An,T. Habib,S. Shah,H. Gao,M. Radovic,M. J. Green,J. L. Lutkenhaus, *Science advances* **2018,** *4*, eaaq0118.

53. D. VietáDao, *RSC Advances* **2015,** *5*, 82121.

54. J. T. Muth,D. M. Vogt,R. L. Truby,Y. Mengüç,D. B. Kolesky,R. J. Wood,J. A. Lewis, *Advanced Materials* **2014,** *26*, 6307.

55. C. B. Cooper,K. Arutselvan,Y. Liu,D. Armstrong,Y. Lin,M. R. Khan,J. Genzer,M. D. Dickey, *Advanced Functional Materials* **2017,** *27*, 1605630.

56. H. Ota,K. Chen,Y. Lin,D. Kiriya,H. Shiraki,Z. Yu,T.-J. Ha,A. Javey, *Nature communications* **2014,** *5*, 5032.

57. X.-Y. Yin,Y. Zhang,X. Cai,Q. Guo,J. Yang,Z. L. Wang, *Materials Horizons* **2019,** *6*, 767.

58. Y. Jiao,C. W. Young,S. Yang,S. Oren,H. Ceylan,S. Kim,K. Gopalakrishnan,P. C. Taylor,L. Dong, *IEEE Sensors Journal* **2016,** *16*, 7870.

59. A. Hirsch,H. O. Michaud,A. P. Gerratt,S. De Mulatier,S. P. Lacour, *Advanced Materials* **2016,** *28*, 4507.

60. R. Matsuzaki,K. Tabayashi, *Advanced Functional Materials* **2015,** *25*, 3806.

61. J.-B. Chossat,Y.-L. Park,R. J. Wood,V. Duchaine, *IEEE Sensors Journal* **2013,** *13*, 3405.

62. C. Liu,S. Han,H. Xu,J. Wu,C. Liu, *ACS applied materials & interfaces* **2018,** *10*, 31716.

63. M. Xu,J. Qi,F. Li,Y. Zhang, *Nanoscale* **2018,** *10*, 5264.

64. Q. Liu,J. Chen,Y. Li,G. Shi, *ACS nano* **2016,** *10*, 7901.

65. G. Shi,Z. Zhao,J. H. Pai,I. Lee,L. Zhang,C. Stevenson,K. Ishara,R. Zhang,H. Zhu,J. Ma, *Advanced Functional Materials* **2016,** *26*, 7614.

66. X. Shi,S. Liu,Y. Sun,J. Liang,Y. Chen, *Advanced Functional Materials* **2018,** *28*, 1800850.

67. D. Kim,S. K. Ahn,J. Yoon, *Advanced Materials Technologies* **2019**, 1800739.

68. S. Chen,H. Liu,S. Liu,P. Wang,S. Zeng,L. Sun,L. Liu, *ACS applied materials & interfaces* **2018,** *10*, 4305.

69. J. Sun,Y. Zhao,Z. Yang,J. Shen,E. Cabrera,M. J. Lertola,W. Yang,D. Zhang,A. Benatar,J. M. Castro, *Nanotechnology* **2018,** *29*, 355304.

70. Z. Tang,S. Jia,F. Wang,C. Bian,Y. Chen,Y. Wang,B. Li, *ACS applied materials & interfaces* **2018,** *10*, 6624.

71. Y.-F. Yang,L.-Q. Tao,Y. Pang,H. Tian,Z.-Y. Ju,X.-M. Wu,Y. Yang,T.-L. Ren, *Nanoscale* **2018,** *10*, 11524.

72. G. Hassan,J. Bae,A. Hassan,S. Ali,C. H. Lee,Y. Choi, *Composites Part A: Applied Science and Manufacturing* **2018,** *107*, 519.

73. F. Yin,J. Yang,P. Ji,H. Peng,Y. Tang,W. Yuan, *ACS applied materials & interfaces* **2019**.

74. J. Oh,J. C. Yang,J.-O. Kim,H. Park,S. Y. Kwon,S. Lee,J. Y. Sim,H. W. Oh,J. Kim,S. Park, *ACS nano* **2018,** *12*, 7546.

75. S. Wang,P. Xiao,Y. Liang,J. Zhang,Y. Huang,S. Wu,S.-W. Kuo,T. Chen, *Journal of Materials Chemistry C* **2018,** *6*, 5140.

76. S. R. Larimi,H. R. Nejad,M. Oyatsi,A. O'Brien,M. Hoorfar,H. Najjaran, *Sensors and Actuators A: Physical* **2018,** *271*, 182.

77. X. Wang,J. Li,H. Song,H. Huang,J. Gou, *ACS applied materials & interfaces* **2018,** *10*, 7371.

78. X. Zhou,L. Zhu,L. Fan,H. Deng,Q. Fu, *ACS applied materials & interfaces* **2018,** *10*, 31655.

79. N. Gupta,K. D. M. Rao,K. Srivastava,R. Gupta,A. Kumar,A. Marconnet,T. S. Fisher,G. U. Kulkarni, *ACS applied materials & interfaces* **2018,** *10*, 44126.

80. M. Amjadi,M. Turan,C. P. Clementson,M. Sitti, *ACS applied materials & interfaces* **2016,** *8*, 5618.

81. Z. Wang,L. Zhang,J. Liu,C. Li, *ACS applied materials & interfaces* **2018,** *11*, 5316.

82. X. Liao,Z. Zhang,Z. Kang,F. Gao,Q. Liao,Y. Zhang, *Materials Horizons* **2017,** *4*, 502.

83. S. Gong,D. T. Lai,Y. Wang,L. W. Yap,K. J. Si,Q. Shi,N. N. Jason,T. Sridhar,H. Uddin,W. Cheng, *ACS applied materials & interfaces* **2015,** *7*, 19700.

84. S. Gong,D. T. Lai,B. Su,K. J. Si,Z. Ma,L. W. Yap,P. Guo,W. Cheng, *Advanced Electronic Materials* **2015,** *1*, 1400063.

85. A. Chortos,J. Lim,J. W. To,M. Vosgueritchian,T. J. Dusseault,T. H. Kim,S. Hwang,Z. Bao, *Advanced Materials* **2014,** *26*, 4253.

86. Z. Song,W. Li,Y. Bao,F. Han,L. Gao,J. Xu,Y. Ma,D. Han,L. Niu, *ACS applied materials & interfaces* **2018,** *10*, 42826.

87. J. Liu,F. Zhao,Q. Tao,J. Cao,Y. Yu,X. Zhang, *Materials Horizons* **2019**.

88. P. Lee,J. Lee,H. Lee,J. Yeo,S. Hong,K. H. Nam,D. Lee,S. S. Lee,S. H. Ko, *Advanced materials* **2012,** *24*, 3326.

89. H. Kim,H. Lee,I. Ha,J. Jung,P. Won,H. Cho,J. Yeo,S. Hong,S. Han,J. Kwon, *Advanced Functional Materials* **2018,** *28*, 1801847.

90. J. H. Park,S. Han,D. Kim,B. K. You,D. J. Joe,S. Hong,J. Seo,J. Kwon,C. K. Jeong,H. J. Park, *Advanced Functional Materials* **2017,** *27*, 1701138.

91. T. Park,I. Chang,J. H. Jung,H. B. Lee,S. H. Ko,R. O'Hayre,S. J. Yoo,S. W. Cha, *Energy* **2017,** *134*, 412.

92. I. Chang,T. Park,J. Lee,M. H. Lee,S. H. Ko,S. W. Cha, *Journal of Materials Chemistry A* **2013,** *1*, 8541.

93. F. Yin,J. Yang,H. Peng,W. Yuan, *Journal of Materials Chemistry C* **2018,** *6*, 6840.

94. X.-P. Li,Y. Li,X. Li,D. Song,P. Min,C. Hu,H.-B. Zhang,N. Koratkar,Z.-Z. Yu, *Journal of colloid and interface science* **2019,** *542*, 54.

95. J. Li,S. Orrego,J. Pan,P. He,S. H. Kang, *Nanoscale* **2019,** *11*, 2779.

96. A. Tewari,S. Gandla,S. Bohm,C. R. McNeill,D. Gupta, *ACS applied materials & interfaces* **2018,** *10*, 5185.

97. M. Liu,X. Pu,C. Jiang,T. Liu,X. Huang,L. Chen,C. Du,J. Sun,W. Hu,Z. L. Wang, *Advanced Materials* **2017,** *29*, 1703700.

98. Y. Yue,N. Liu,W. Liu,M. Li,Y. Ma,C. Luo,S. Wang,J. Rao,X. Hu,J. Su, *Nano energy* **2018,** *50*, 79.

99. J. Y. Yoo,M. H. Seo,J. S. Lee,K. W. Choi,M. S. Jo,J. B. Yoon, *Advanced Functional Materials* **2018,** *28*, 1804721.

100. Y. Gao,C. Lu,Y. Guohui,J. Sha,J. Tan,F. Xuan, *Nanotechnology* **2019,** *30*, 325502.

101. J. Jia,G. Huang,J. Deng,K. Pan, *Nanoscale* **2019,** *11*, 4258.

102. P. Wei,H. Leng,Q. Chen,R. Advincula,E. B. Pentzer, *ACS Applied Polymer Materials* **2019**.

103. Z. Yue,X. Ye,S. Liu,Y. Zhu,H. Jiang,Z. Wan,Y. Lin,C. Jia, *Biosensors and Bioelectronics* **2019,** *139*, 111296.

104. S. Han,C. Liu,Z. Huang,J. Zheng,H. Xu,S. Chu,J. Wu,C. Liu, *Advanced Materials Technologies* **2019**, 1800640.

105. Q. J. Sun,X. H. Zhao,Y. Zhou,C. C. Yeung,W. Wu,S. Venkatesh,Z. X. Xu,J. J. Wylie,W. J. Li,V. A. Roy, *Advanced Functional Materials* **2019**, 1808829.

106. L. Yang,Y. Liu,C. D. Filipe,D. Ljubic,Y. Luo,H. Zhu,J. Yan,S. Zhu, *ACS applied materials & interfaces* **2019,** *11*, 4318.

107. Z. Chen,Y. Hu,H. Zhuo,L. Liu,S. Jing,L. Zhong,X. Peng,R.-c. Sun, *Chemistry of Materials* **2019**.

108. Y. Hu,H. Zhuo,Q. Luo,Y. Wu,R. Wen,Z. Chen,L. Liu,L. Zhong,X. Peng,R. Sun, *Journal of Materials Chemistry A* **2019,** *7*, 10273.

109. Z. Xiao,W. Zhou,N. Zhang,Q. Zhang,X. Xia,X. Gu,Y. Wang,S. Xie, *Small* **2019**, 1804779.

110. T. Li,L. Li,Y. Bai,Y. Cao,Q. Lu,Y. Li,G. Xu,T. Zhang, *Nanoscale* **2019**.

111. S. J. Park,J. Kim,M. Chu,M. Khine, *Advanced Materials Technologies* **2018,** *3*, 1700158.

112. Z. Wang,L. Zhang,J. Liu,H. Jiang,C. Li, *Nanoscale* **2018,** *10*, 10691.

113. Z. He,W. Chen,B. Liang,C. Liu,L. Yang,D. Lu,Z. Mo,H. Zhu,Z. Tang,X. Gui, *ACS applied materials & interfaces* **2018,** *10*, 12816.

114. H. Nesser,J. Grisolia,T. Alnasser,B. Viallet,L. Ressier, *Nanoscale* **2018,** *10*, 10479.

115. A. Frutiger,J. T. Muth,D. M. Vogt,Y. Mengüç,A. Campo,A. D. Valentine,C. J. Walsh,J. A. Lewis, *Advanced Materials* **2015,** *27*, 2440.

116. A. Atalay,V. Sanchez,O. Atalay,D. M. Vogt,F. Haufe,R. J. Wood,C. J. Walsh, *Advanced Materials Technologies* **2017,** *2*, 1700136.

117. S.-R. Kim,J.-H. Kim,J.-W. Park, *ACS applied materials & interfaces* **2017,** *9*, 26407.

118. O. Atalay,A. Atalay,J. Gafford,H. Wang,R. Wood,C. Walsh, *Advanced Materials Technologies* **2017,** *2*, 1700081.

119. H. Xu,Y. Lv,D. Qiu,Y. Zhou,H. Zeng,Y. Chu, *Nanoscale* **2019,** *11*, 1570.

120. J. Zhang,L. Wan,Y. Gao,X. Fang,T. Lu,L. Pan,F. Xuan, *Advanced Electronic Materials* **2019**, 1900285.

121. S. Yao,L. Vargas,X. Hu,Y. Zhu, *IEEE Sensors Journal* **2018,** *18*, 3010.

122. J. Kim,E. F. Chou,J. Le,S. Wong,M. Chu,M. Khine, *Advanced healthcare materials* **2019**, 1900109.

123. S. Chen,S. Peng,W. Sun,G. Gu,Q. Zhang,X. Guo, *Advanced Materials Technologies* **2019**, 1800681.

124. J. Yang,S. Luo,X. Zhou,J. Li,J. Fu,W. Yang,D. Wei, *ACS applied materials & interfaces* **2019,** *11*, 14997.

125. C. Hou,Z. Xu,W. Qiu,R. Wu,Y. Wang,Q. Xu,X. Y. Liu,W. Guo, *Small* **2019,** *15*, 1805084.

126. W. Yang,N. W. Li,S. Zhao,Z. Yuan,J. Wang,X. Du,B. Wang,R. Cao,X. Li,W. Xu, *Advanced Materials Technologies* **2018,** *3*, 1700241.

127. X. Zeng,Z. Wang,H. Zhang,W. Yang,L. Xiang,Z. Zhao,L.-M. Peng,Y. Hu, *ACS applied materials & interfaces* **2019**.

128. Y. Wan,Z. Qiu,Y. Hong,Y. Wang,J. Zhang,Q. Liu,Z. Wu,C. F. Guo, *Advanced Electronic Materials* **2018,** *4*, 1700586.

129. H. Shi,M. Al-Rubaiai,C. M. Holbrook,J. Miao,T. Pinto,C. Wang,X. Tan, *Advanced Functional Materials* **2019**, 1809116.

130. H. Kim,G. Kim,T. Kim,S. Lee,D. Kang,M. S. Hwang,Y. Chae,S. Kang,H. Lee,H. G. Park, *Small* **2018,** *14*, 1703432.

131. Y. Luo,J. Shao,S. Chen,X. Chen,H. Tian,X. Li,L. Wang,D. Wang,B. Lu, *ACS applied materials & interfaces* **2019**.

132. J. Wang,R. Suzuki,M. Shao,F. Gillot,S. Shiratori, *ACS applied materials & interfaces* **2019,** *11*, 11928.

133. D. Kwon,T.-I. Lee,J. Shim,S. Ryu,M. S. Kim,S. Kim,T.-S. Kim,I. Park, *ACS applied materials & interfaces* **2016,** *8*, 16922.

134. A. Chortos,J. Liu,Z. Bao, *Nature materials* **2016,** *15*, 937.

135. S. C. Mannsfeld,B. C. Tee,R. M. Stoltenberg,C. V. H. Chen,S. Barman,B. V. Muir,A. N. Sokolov,C. Reese,Z. Bao, *Nature materials* **2010,** *9*, 859.

136. S. Y. Kim,S. Park,H. W. Park,D. H. Park,Y. Jeong,D. H. Kim, *Advanced materials* **2015,** *27*, 4178.

137. J. Y. Sun,C. Keplinger,G. M. Whitesides,Z. Suo, *Advanced Materials* **2014,** *26*, 7608.

138. B. Nie,R. Huang,T. Yao,Y. Zhang,Y. Miao,C. Liu,J. Liu,X. Chen, *Advanced Functional Materials* **2019**, 1808786.

139. L. Song,A. C. Myers,J. J. Adams,Y. Zhu, *ACS applied materials & interfaces* **2014,** *6*, 4248.

140. S. Cheng,Z. Wu, *Advanced Functional Materials* **2011,** *21*, 2282.

141. H. J. Koo,J. H. So,M. D. Dickey,O. D. Velev, *Advanced materials* **2011,** *23*, 3559.

142. T. N. Do,Y. Visell, *Scientific reports* **2017,** *7*, 1753.

143. J. Fastier-Wooller,T. Dinh,V. T. Dau,D. V. Dao, *RSC advances* **2019,** *9*, 10733.

144. M. D. Dickey, *Advanced Materials* **2017,** *29*, 1606425.

145. T. W. Clarkson,L. Magos, *Critical reviews in toxicology* **2006,** *36*, 609.

146. S. Zhu,J. H. So,R. Mays,S. Desai,W. R. Barnes,B. Pourdeyhimi,M. D. Dickey, *Advanced Functional Materials* **2013,** *23*, 2308.

147. N. Kazem,T. Hellebrekers,C. Majidi, *Advanced Materials* **2017,** *29*, 1605985.

148. A. Tabatabai,A. Fassler,C. Usiak,C. Majidi, *Langmuir* **2013,** *29*, 6194.

149. J. B. Andrews,K. Mondal,T. V. Neumann,J. A. Cardenas,J. Wang,D. P. Parekh,Y. Lin,P. Ballentine,M. D. Dickey,A. D. Franklin, *ACS nano* **2018,** *12*, 5482.

150. S. Cheng,A. Rydberg,K. Hjort,Z. Wu, *Applied Physics Letters* **2009,** *94*, 144103.

151. S. Cheng,Z. Wu,P. Hallbjorner,K. Hjort,A. Rydberg, *IEEE Transactions on antennas and propagation* **2009,** *57*, 3765.

152. M. Kubo,X. Li,C. Kim,M. Hashimoto,B. J. Wiley,D. Ham,G. M. Whitesides, *Advanced materials* **2010,** *22*, 2749.

153. I. D. Joshipura,H. R. Ayers,C. Majidi,M. D. Dickey, *Journal of materials chemistry c* **2015,** *3*, 3834.

154. M. G. Mohammed,R. Kramer, *Advanced Materials* **2017,** *29*, 1604965.

155. C. W. Park,Y. G. Moon,H. Seong,S. W. Jung,J.-Y. Oh,B. S. Na,N.-M. Park,S. S. Lee,S. G. Im,J. B. Koo, *ACS applied materials & interfaces* **2016,** *8*, 15459.

156. C. Pan,K. Kumar,J. Li,E. J. Markvicka,P. R. Herman,C. Majidi, *Advanced Materials* **2018,** *30*, 1706937.

157. G. Li,X. Wu,D.-W. Lee, *Sensors and Actuators B: Chemical* **2015,** *221*, 1114.

158. C. Yang,Z. Suo, *Nature Reviews Materials* **2018,** *3*, 125.

159. C. Keplinger,J.-Y. Sun,C. C. Foo,P. Rothemund,G. M. Whitesides,Z. Suo, *Science* **2013,** *341*, 984.

160. C.-C. Kim,H.-H. Lee,K. H. Oh,J.-Y. Sun, *Science* **2016,** *353*, 682.

161. S. Zhang,F. Wang,H. Peng,J. Yan,G. Pan, *ACS Omega* **2018,** *3*, 3014.

162. S. Savagatrup,E. Chan,S. M. Renteria-Garcia,A. D. Printz,A. V. Zaretski,T. F. O'Connor,D. Rodriquez,E. Valle,D. J. Lipomi, *Advanced Functional Materials* **2015,** *25*, 427.

163. T. Q. Trung,S. Ramasundaram,B. U. Hwang,N. E. Lee, *Advanced materials* **2016,** *28*, 502.

164. M. M. Voigt,R. C. Mackenzie,C. P. Yau,P. Atienzar,J. Dane,P. E. Keivanidis,D. D. Bradley,J. Nelson, *Solar Energy Materials and Solar Cells* **2011,** *95*, 731.

165. Y. Wang,C. Zhu,R. Pfattner,H. Yan,L. Jin,S. Chen,F. Molina-Lopez,F. Lissel,J. Liu,N. I. Rabiah, *Science advances* **2017,** *3*, e1602076.

166. J. Y. Oh,S. Kim,H. K. Baik,U. Jeong, *Advanced Materials* **2016,** *28*, 4455.

167. M. Vosgueritchian,D. J. Lipomi,Z. Bao, *Advanced functional materials* **2012,** *22*, 421.

168. R. Po,C. Carbonera,A. Bernardi,F. Tinti,N. Camaioni, *Solar Energy Materials and Solar Cells* **2012,** *100*, 97.

169. L. V. Kayser,M. D. Russell,D. Rodriquez,S. N. Abuhamdieh,C. Dhong,S. Khan,A. N. Stein,J. Ramírez,D. J. Lipomi, *Chemistry of Materials* **2018,** *30*, 4459.

170. S. G. R. Bade,X. Shan,P. T. Hoang,J. Li,T. Geske,L. Cai,Q. Pei,C. Wang,Z. Yu, *Advanced Materials* **2017,** *29*, 1607053.

171. G. Yun,S.-Y. Tang,S. Sun,D. Yuan,Q. Zhao,L. Deng,S. Yan,H. Du,M. D. Dickey,W. Li, *Nature communications* **2019,** *10*, 1300.

172. Y. Lu,M. C. Biswas,Z. Guo,J.-W. Jeon,E. K. Wujcik, *Biosensors and Bioelectronics* **2018**.

173. T. Dinh,T.-K. Nguyen,H.-P. Phan,J. Fastier-Wooller,C.-D. Tran,N.-T. Nguyen,D. V. Dao, *IEEE Electron Device Letters* **2018,** *39*, 584.

174. L. Chen,G. Chen,L. Lu, *Advanced Functional Materials* **2007,** *17*, 898.

175. L. Groenendaal,F. Jonas,D. Freitag,H. Pielartzik,J. R. Reynolds, *Advanced materials* **2000,** *12*, 481.

176. M. Amjadi,K. U. Kyung,I. Park,M. Sitti, *Advanced Functional Materials* **2016,** *26*, 1678.

177. S.-H. Bae,Y. Lee,B. K. Sharma,H.-J. Lee,J.-H. Kim,J.-H. Ahn, *Carbon* **2013,** *51*, 236.

178. Y. Qin,Q. Peng,Y. Ding,Z. Lin,C. Wang,Y. Li,F. Xu,J. Li,Y. Yuan,X. He, *ACS nano* **2015,** *9*, 8933.

179. T. Jiang,R. Huang,Y. Zhu, *Advanced Functional Materials* **2014,** *24*, 396.

180. S. J. Park,J. Kim,M. Chu,M. Khine, *Advanced Materials Technologies* **2016,** *1*, 1600053.

181. T. Dinh,H.-P. Phan,T.-K. Nguyen,A. Qamar,A. R. M. Foisal,T. N. Viet,C.-D. Tran,Y. Zhu,N.-T. Nguyen,D. V. Dao, *Journal of Materials Chemistry C* **2016,** *4*, 10061.

182. T.-K. Nguyen,T. Dinh,H.-P. Phan,C.-D. Tran,A. R. M. Foisal,Y. Zhu,D. V. Dao, *IEEE Electron Device Letters* **2017,** *38*, 1331.

183. J. L. Abot,T. Alosh,K. Belay, *Carbon* **2014,** *70*, 95.

184. J. Zhou,H. Yu,X. Xu,F. Han,G. Lubineau, *ACS applied materials & interfaces* **2017,** *9*, 4835.

185. C. Yan,J. Wang,W. Kang,M. Cui,X. Wang,C. Y. Foo,K. J. Chee,P. S. Lee, *Advanced materials* **2014,** *26*, 2022.

186. S. W. Lee,J. J. Park,B. H. Park,S. C. Mun,Y. T. Park,K. Liao,T. S. Seo,W. J. Hyun,O. O. Park, *ACS applied materials & interfaces* **2017,** *9*, 11176.

187. L.-Q. Tao,D.-Y. Wang,H. Tian,Z.-Y. Ju,Y. Liu,Y. Pang,Y.-Q. Chen,Y. Yang,T.-L. Ren, *Nanoscale* **2017,** *9*, 8266.

188. J. Zhao,C. He,R. Yang,Z. Shi,M. Cheng,W. Yang,G. Xie,D. Wang,D. Shi,G. Zhang, *Applied Physics Letters* **2012,** *101*, 063112.

189. C. K. Jeong,J. Lee,S. Han,J. Ryu,G. T. Hwang,D. Y. Park,J. H. Park,S. S. Lee,M. Byun,S. H. Ko, *Advanced materials* **2015,** *27*, 2866.

190. J. Kwon,Y. D. Suh,J. Lee,P. Lee,S. Han,S. Hong,J. Yeo,H. Lee,S. H. Ko, *Journal of Materials Chemistry C* **2018,** *6*, 7445.

191. S. Hong,H. Lee,J. Lee,J. Kwon,S. Han,Y. D. Suh,H. Cho,J. Shin,J. Yeo,S. H. Ko, *Advanced materials* **2015,** *27*, 4744.

192. J. H. Cho,S.-H. Ha,J.-M. Kim, *Nanotechnology* **2018,** *29*, 155501.

193. H. Jeong,Y. Noh,S. H. Ko,D. Lee, *Composites Science and Technology* **2019,** *174*, 50.

194. S. Lee,S. Shin,S. Lee,J. Seo,J. Lee,S. Son,H. J. Cho,H. Algadi,S. Al-Sayari,D. E. Kim, *Advanced Functional Materials* **2015,** *25*, 3114.

195. N. Matsuhisa,D. Inoue,P. Zalar,H. Jin,Y. Matsuba,A. Itoh,T. Yokota,D. Hashizume,T. Someya, *Nature materials* **2017,** *16*, 834.

196. M. Park,J. Im,M. Shin,Y. Min,J. Park,H. Cho,S. Park,M.-B. Shim,S. Jeon,D.-Y. Chung, *Nature nanotechnology* **2012,** *7*, 803.

197. K. K. Kim,I. Ha,P. Won,D.-G. Seo,K.-J. Cho,S. H. Ko, *Nature communications* **2019,** *10*, 2582.

198. D. Kim,J. Kwon,J. Jung,K. Kim,H. Lee,J. Yeo,S. Hong,S. Han,S. H. Ko, *Small Methods* **2018,** *2*, 1800077.

199. I. Hong,S. Lee,D. Kim,H. Cho,Y. Roh,H. An,S. Hong,S. H. Ko,S. Han, *Nanotechnology* **2018,** *30*, 074001.

200. H. S. Jo,S. An,C.-W. Park,D.-Y. Woo,A. L. Yarin,S. S. Yoon, *ACS Applied Materials & Interfaces* **2019**.

201. H. S. Jo,H.-J. Kwon,T.-G. Kim,C.-W. Park,S. An,A. L. Yarin,S. S. Yoon, *Nanoscale* **2018,** *10*, 19825.

202. S. G. Yoon,H.-J. Koo,S. T. Chang, *ACS applied materials & interfaces* **2015,** *7*, 27562.

203. N. Liu,G. Fang,J. Wan,H. Zhou,H. Long,X. Zhao, *Journal of Materials Chemistry* **2011,** *21*, 18962.

204. B. Sun,Y.-Z. Long,S.-L. Liu,Y.-Y. Huang,J. Ma,H.-D. Zhang,G. Shen,S. Xu, *Nanoscale* **2013,** *5*, 7041.

205. N. Hu,Y. Karube,M. Arai,T. Watanabe,C. Yan,Y. Li,Y. Liu,H. Fukunaga, *Carbon* **2010,** *48*, 680.

206. N. Hu,Y. Karube,C. Yan,Z. Masuda,H. Fukunaga, *Acta Materialia* **2008,** *56*, 2929.

207. K. Huang,S. Dong,J. Yang,J. Yan,Y. Xue,X. You,J. Hu,L. Gao,X. Zhang,Y. Ding, *Carbon* **2019,** *143*, 63.

208. W. Tang,T. Yan,F. Wang,J. Yang,J. Wu,J. Wang,T. Yue,Z. Li, *Carbon* **2019,** *147*, 295.

209. Y. Cai,J. Shen,G. Ge,Y. Zhang,W. Jin,W. Huang,J. Shao,J. Yang,X. Dong, *ACS nano* **2017,** *12*, 56.

210. Y. Ma,Y. Yue,H. Zhang,F. Cheng,W. Zhao,J. Rao,S. Luo,J. Wang,X. Jiang,Z. Liu, *ACS nano* **2018,** *12*, 3209.

211. A. S. Almuslem,S. F. Shaikh,M. M. Hussain, *Advanced Materials Technologies* **2019**, 1900145.

212. T. Dinh,H.-P. Phan,T.-K. Nguyen,V. Balakrishnan,H.-H. Cheng,L. Hold,A. Lacopi,N.-T. Nguyen,D. V. Dao, *IEEE Electron Device Letters* **2018,** *39*, 580.

213. T. Dinh,D. V. Dao,H.-P. Phan,L. Wang,A. Qamar,N.-T. Nguyen,P. Tanner,M. Rybachuk, *Applied Physics Express* **2015,** *8*, 061303.

214. M. Peters,J. Kumpfert,C. H. Ward,C. Leyens, *Advanced engineering materials* **2003,** *5*, 419.

215. T. Dinh,H.-P. Phan,A. Qamar,P. Woodfield,N.-T. Nguyen,D. V. Dao, *Journal of Microelectromechanical Systems* **2017,** *26*, 966.

216. T. Dinh,T. K. Nguyen,H. P. Phan,Q. Nguyen,J. Han,S. Dimitrijev,N. T. Nguyen,D. V. Dao, *Advanced Engineering Materials* **2019,** *21*, 1801049.

217. P. Wang,L. Cheng,Y. Zhang,H. Wu,Y. Hou,W. Yuan,L. Zheng, *Ceramics International* **2017,** *43*, 7424.

218. S. Chen,M. Shang,F. Gao,L. Wang,P. Ying,W. Yang,X. Fang, *Advanced Science* **2016,** *3*, 1500256.

219. C.-H. Cheng,A.-J. Tzou,J.-H. Chang,Y.-C. Chi,Y.-H. Lin,M.-H. Shih,C.-K. Lee,C.-I. Wu,H.-C. Kuo,C.-Y. Chang, *Scientific reports* **2016,** *6*, 19757.